Impacts of climate change on surface ozone and intercontinental ozone pollution: A multi-model study

R. M. Doherty,[1] O. Wild,[2] D. T. Shindell,[3] G. Zeng,[4] I. A. MacKenzie,[1] W. J. Collins,[5,12] A. M. Fiore,[6,13] D. S. Stevenson,[1] F. J. Dentener,[7] M. G. Schultz,[8] P. Hess,[9] R. G. Derwent,[10] and T. J. Keating[11]

Received 18 July 2012; revised 8 February 2013; accepted 8 February 2013; published 7 May 2013.

[1] The impact of climate change between 2000 and 2095 SRES A2 climates on surface ozone $(O)_3$ and on O_3 source-receptor (S-R) relationships is quantified using three coupled climate-chemistry models (CCMs). The CCMs exhibit considerable variability in the spatial extent and location of surface O_3 increases that occur within parts of high NO_x emission source regions (up to 6 ppbv in the annual average and up to 14 ppbv in the season of maximum O_3). In these source regions, all three CCMs show a positive relationship between surface O_3 change and temperature change. Sensitivity simulations show that a combination of three individual chemical processes—(i) enhanced PAN decomposition, (ii) higher water vapor concentrations, and (iii) enhanced isoprene emission—largely reproduces the global spatial pattern of annual-mean surface O_3 response due to climate change ($R^2 = 0.52$). Changes in climate are found to exert a stronger control on the annual-mean surface O_3 response through changes in climate-sensitive O_3 chemistry than through changes in transport as evaluated from idealized CO-like tracer concentrations. All three CCMs exhibit a similar spatial pattern of annual-mean surface O_3 change to 20% regional O_3 precursor emission reductions under future climate compared to the same emission reductions applied under present-day climate. The surface O_3 response to emission reductions is larger over the source region and smaller downwind in the future than under present-day conditions. All three CCMs show areas within Europe where regional emission reductions larger than 20% are required to compensate climate change impacts on annual-mean surface O_3.

Citation: Doherty, R. M., et al. (2013), Impacts of climate change on surface ozone and intercontinental ozone pollution: A multi-model study, *J. Geophys. Res. Atmos.*, *118*, 3744–3763, doi:10.1002/jgrd.50266.

1. Introduction

[2] Changes in climate are expected to influence future levels of surface ozone (O_3), a strong oxidant which has adverse impacts on health and ecosystems. Surface O_3 is a local and regional pollutant which typically has peak episodes in spring and summer due to photochemical production. The long lifetime of O_3 with respect to intercontinental transport timescales means that its influence on air quality can also be considered global [*Akimoto*, 2003; *Holloway et al.*, 2003], and rising background O_3 levels recorded at long-term measurement stations [e.g., *Parrish et al.*, 2012] are of concern to policy makers. To determine the effectiveness of O_3 precursor emission controls, the impacts and uncertainty in the O_3 response to climate change need to be evaluated.

Additional supporting information may be found in the online version of this article.

[1]School of GeoSciences, University of Edinburgh, UK.
[2]Lancaster Environment Centre, Lancaster University, Lancaster, UK.
[3]NASA Goddard Institute for Space Studies and Columbia University, New York, New York, USA.
[4]National Institute of Water and Atmospheric Research, Lauder, New Zealand.
[5]Met Office Hadley Centre, Exeter, UK.
[6]NOAA Geophysical Fluid Dynamics Laboratory, Princeton, New Jersey, USA.
[7]European Commission, Joint Research Centre JRC, Institute for Environment and Sustainability, Ispra, Italy.
[8]Institut für Energie- und Klimaforschung—Troposphäre (IEK-8), Forschungszentrum-Jülich, Germany.
[9]Cornell University, Ithaca, New York, USA.
[10]rdscientific, Newbury, Berkshire, UK.
[11]Office of Policy Analysis and Review, Environmental Protection Agency, Washington, DC, USA.
[12]Department of Meteorology, University of Reading, Reading, UK.
[13]Department of Earth and Environmental Sciences, Lamont-Doherty Earth Observatory, Columbia University, Palisades, New York, USA.

Corresponding author: R. Doherty, School of GeoSciences, University of Edinburgh, UK. (ruth.doherty@ed.ac.uk)

©2013. American Geophysical Union. All Rights Reserved.
2169-897X/13/10.1002/jgrd.50266

[3] Changes in climate at global and regional scales will modify the chemical environment and pollutant lifetimes and hence the concentrations of pollutants over source regions and over downwind continents [*Task Force on Hemispheric Transport of Air Pollution* (*TF-HTAP*), 2011]. Changes in climate may also affect meteorological transport processes and hence alter the export and import of pollution. Previous studies suggest that the response of O_3 to climate change in polluted regions differs from that in remote regions [*Murazaki and Hess*, 2006]. In polluted regions, a positive O_3-temperature relationship has been reported from both observational and model studies [*Jacob and Winner*, 2009]. *Bloomer et al*. [2009] define a climate penalty factor as the slope of the O_3-temperature relationship for percentiles of hourly O_3 measurements over 21 years, which ranges between 2.2 and 3.2 ppbv/°C across the rural eastern US depending on emissions of NO_x ($NO + NO_2$). Coupled climate-chemistry model (CCM) studies also show increased surface O_3 associated with climate change in parts of major emission regions [e.g., *Hauglustaine et al*., 2005; *Murazaki and Hess*, 2006; *Racherla and Adams*, 2008; *Wu et al*., 2008; *Royal Society*, 2008; *Jacob and Winner*, 2009]. *Wu et al*. [2008] define a climate penalty more broadly as the need for stronger emission controls to achieve a given air quality standard in a future climate. They find a climate penalty (O_3 increase due to climate change) of 2–5 ppbv in summer daily maximum 8 hour O_3 in the northeastern United States for climate change in the 2050s compared to the 2000s following the SRES A1B scenario. They attribute this increased O_3 to a number of meteorological variables including temperature (a rise of 1–3°C) and mid-latitude cyclone frequency as well as increased biogenic isoprene emission.

[4] The influence of climate change on O_3 and its precursors occurs through multiple processes [e.g., *Jacob and Winner*, 2009; *Isaksen et al*., 2009; *Fiore et al*., 2012]. Changes in temperature and water vapor alter the chemical environment and therefore affect the rates of chemical reactions that create and remove O_3. Many chemical reaction rates increase with temperature, e.g., methane and non-methane hydrocarbon (NMVOC) oxidation rates, and lead to increased O_3 production. In particular, thermal decomposition of peroxyacetylnitrate (PAN), a major reservoir species for long range transport of the O_3 precursors NO_x and HO_x ($OH + HO_2$), increases strongly with increasing temperature. Hence, increases in temperature will decrease the lifetime of PAN and contribute to reduced export of NO_y (total oxidized nitrogen) and thus alter the long-range transport of O_3 pollution [e.g., *Schultz et al*., 1998]. Increased water vapor in a future warmer atmosphere will lead to increased O_3 destruction and shorter O_3 lifetimes [*Johnson et al*., 1999]. This is a robust feature of a previous multi-model study [*Stevenson et al*., 2006]. Amongst other influences on the tropospheric budget of O_3, this may cause a reduction in the contribution of Asian emissions to background O_3 over the United States [*Murazaki and Hess*, 2006; *Lin et al*., 2008]. However, in highly polluted regions, increased water vapor has competing effects on O_3 production [*Jacob and Winner*, 2009].

[5] Climate change may also modify the future chemical environment through changes in natural emissions. Isoprene is a major O_3 precursor under high NO_x conditions [*Trainer et al*., 1991; *Jacob and Winner*, 2009]. Biogenic emission of isoprene increases strongly with temperature [*Guenther et al*., 1995, 2012]. CCMs that employ interactive temperature-sensitive emission schemes simulate net O_3 production increases with higher isoprene emissions in high NO_x regions but decreases in net O_3 production in low NO_x environments [e.g., *Racherla and Adams*, 2008; *Zeng et al*., 2008]. *Racherla and Adams* [2008] find enhanced isoprene emission in future climate to be the dominant cause of increased summer O_3 chemical production in the eastern United States. However, *Ito et al*. [2009] and *Fiore et al*. [2012] highlight that the sign of the O_3 response to temperature and climate change depends on the assumption of the amount of recycling of NO_x from isoprene nitrates. Furthermore, the extent to which CO_2 inhibition of isoprene emissions in a future higher CO_2 climate may offset temperature-driven emission increases is unclear but may be substantial [*Rosenstiel et al*., 2003; *Arneth et al*., 2007; *Heald et al*., 2009; *Young et al*., 2009]. Other factors such as drought and changes in land cover and land use will modify the spatial pattern and magnitude of isoprene emission [*Sanderson et al*., 2003; *Wu et al*., 2012, *Guenther et al*., 2012]. Another key uncertainty is how dry deposition changes in a warmer climate [*Andersson and Engardt*, 2010; *Wu et al*., 2012] and in particular in regions where warming is likely to be accompanied by drying, such as in the sub-tropics [*Held and Soden*, 2006]. Lastly, changes in cloud extent and properties as well as in precipitation will affect O_3 production from lightning and also influence photolysis rates and wet deposition of nitric acid (HNO_3), the main NO_x sink.

[6] Meteorological transport pathways for pollutants may also be modified in a future climate through changes in synoptic and convective transport. A number of studies have suggested future decreases in synoptic-scale circulation frequency leading to increased summertime surface O_3 pollution episodes over the eastern United States and Europe [*Mickley et al*., 2004; *Forkel and Knoche*, 2006; *Murazaki and Hess*, 2006; *Leibensperger et al*., 2008; *Wu et al*., 2008]. These changes in transport generally favor reduced export of pollutants from source regions. However, *Racherla and Adams* [2008] also find increasing O_3 episodes, but neither these authors nor *Lang and Waugh* [2011] find evidence of future changes in synoptic-scale circulation.

[7] This paper focuses on quantifying the impacts of climate change and their associated uncertainty on surface O_3 over its source regions and over downwind continents, hereafter termed source-receptor (S-R) relationships as in *Fiore et al*. [2011, 2009] and [*TF-HTAP*, 2007, 2011]. It builds on the approach used in multi-model experiments coordinated by the Task Force on Hemispheric Transport of Air Pollutants (TF-HTAP). The Task Force, set up to inform the Convention on Long-range Transboundary Air Pollution (CLRTAP), designed model experiments to quantify source-receptor relationships by performing emission perturbations over four world regions: North America, Europe, East Asia, and South Asia [*Fiore et al*., 2009; *TF-HTAP*, 2007, 2011]. In this study, the model experiments are performed within the context of climate change between the 2000s and 2100s as simulated under the SRES A2 greenhouse gas emissions scenario that yields global surface temperature changes of ~3K between the two periods. Here three CCMs, evaluated in the previous TF-HTAP studies

for O_3 and its precursors [*Sanderson et al*., 2008; *Shindell et al*., 2008; *Fiore et al*., 2009; *Jonson et al*., 2010], are used to quantify the impact of climate change on surface O_3 and on its S-R relationships. This study examines the effect of climate change isolated from the effect of changing future emissions that are addressed in *Wild et al*. [2012]. Hence, the same (present-day) anthropogenic emissions are used in the simulations for "present-day" and "future" climates.

[8] The methodology is described in section 2 and the effects of climate change on surface O_3 and its precursors are discussed in section 3. Section 4 analyzes O_3-temperature-NO_x relationships. Individual key chemical processes influenced by climate change are then examined as well as the influence of climate change on transport (sections 5 and 6). S-R relationships for O_3 are the focus of section 7, and the influence of individual chemical processes on O_3 S-R relationships are outlined in section 8. Section 9 compares the impact of climate change to the impact of anthropogenic emission reductions of O_3 precursors on surface O_3. Overall findings are then presented in section 10.

2. Methodology

[9] Model integrations were performed with three CCMs to examine (a) the influence of climate change on surface O_3 and its precursors and (b) the influence of climate change on intercontinental transport and O_3 S-R relationships for four major emission regions. An additional set of experiments was performed with one CCM to quantify the relative importance of different chemical processes influenced by climate change that impact surface O_3 and its S-R relationships.

2.1. Models and Climate and Emission Reduction Simulations

[10] The influence of climate change on surface O_3 and O_3 S-R relationships is simulated by three CCMs which comprise chemistry transport models coupled to atmospheric general circulation models (AGCMs): GISS-PUCCINI-ModelE (hereafter GISS-PUCCINI), STOC-HadAM3, and UM-CAM. The three CCMs have been widely used [e.g., *Fiore et al*., 2009]. Their grid resolution and chemical, transport, and deposition schemes are outlined in Table S1 in the auxiliary material.

[11] To simulate present-day and future climate, the AGCMs were driven by sea-surface temperatures (SSTs) and sea-ice distributions from previous coupled ocean-atmosphere model integrations that were forced by greenhouse-gas emissions from the SRES A2 emission scenario [*Nakicenovic et al*., 2000]. The SRES A2 scenario was chosen as it lies at the upper end of the magnitude of future projected greenhouse gas emission trends and therefore represents a relatively large climate change signal with concomitant effects on chemistry and transport. In 2100, the SRES A2 scenario has a radiative forcing relative to the pre-industrial (1750) of about 8.1 W m^{-2} [IPCC, 2001], similar to the latest IPCC Representative Concentration Pathways (RCP) 8.5 scenario [*Meinshausen et al*., 2011], which has a radiative forcing of 8.5 W m^{-2}.

[12] The GISS-Model E and HadCM3 GCMs were used to provide SSTs and sea ice for the GISS-PUCCINI and STOC-HadAM3/UM-CAM CCMs, respectively. To ensure that future changes in O_3 and O_3 S-R relationships can be attributed to climate change rather than inter-annual variability, 5 years of simulations were performed. Two base-case integrations were carried out using meteorology from the AGCMs for 2001–2005 and 2095–2099 (Table 1). The 5 year annual-average increase in global-mean surface temperature and specific humidity between present-day and future periods averaged across the three CCMs was 3.0K (range 2.8–3.4K) and 19% (18–21%), respectively. These values are used for perturbation simulations in section 2.3. For GISS-PUCCINI, the 5 year average surface temperature and humidity changes between 2000–2005 and 2095–2099 were compared to differences in 5 year averages separated by 100 years sampled from a 2000 year long unforced control run to provide a comprehensive measure of internal model variability in the absence of climate change. Over much of the world, the surface temperature and humidity changes from the climate change runs examined here are 5 and 30 times greater, respectively, than those due to the unforced internal model variability (Figure S1). It is concluded that the changes in surface temperature and humidity between the 5 year simulations analyzed here

Table 1. Experiments Performed and Their Description Including Number of Simulations and Models Performing Simulations

Experiment Name Used in This Study	HTAP Experiment Name	Description	Number of Models
2000base	FC1	2000–2005 climate based on GCM SSTs	All 3 models: GISS-PUCCINI, STOC-HadAM3, UM-CAM
2095base	FC2	2095–2099 climate based on GCM SSTs	All three models
2000em_NA, EU, EA, SA	FC3NA, EU, EA, SA	Regional emission reductions of NO_x, CO, NMVOCs for 2000–2005 climate for four world regions	All three models
2095em_NA, EU, EA, SA	FC4NA, EU, EA, SA	Regional emission reductions of NO_x, CO, NMVOCs for 2095–2099 climate for four world regions	All three models
2000PAN[a]		2000–2005 climate; added +3K to PAN decomposition rate: $PAN + M = CH_3COO_2 + NO_2 + M$	STOC-HadAM3
2000H2O[a]		2000–2005 climate; multiplied the water vapor concentration by 119%.	STOC-HadAM3
2000ISO[a]		2000–2005 climate; added +3K to isoprene emission scheme	STOC-HadAM3
2000COM[a]		2000–2005 climate; added +3K to PAN decomposition rate and isoprene emission scheme and multiplied the water vapor concentration by 119%.	STOC-HadAM3

[a]For all these experiments, an additional simulation was performed with reduced emissions over the NA source region, i.e., 2000PANem_NA, etc.

are due to climate change and that for these simulations, 5 years is long enough to capture the climate change signal between 2000 and 2095.

[13] To isolate the effects of climate change on O_3 and its S-R relationships, anthropogenic emissions and methane concentrations were held fixed at 2001 values for both present-day and future simulations, as in earlier TF-HTAP experiments [*Fiore et al.*, 2009]. For GISS-PUCCINI, the methane concentrations were fixed at the surface at 1760 ppbv, while for STOC-HADAM3 and UM-CAM, methane concentrations were fixed at 1760 ppbv throughout the model domain. Global emissions totals for NO_x, CO, and NMVOC used in these simulations that include total, anthropogenic, biomass burning, and natural categories are given in Table S2, and the spatial distributions are shown in Figure S2. The three CCMs used similar anthropogenic and biomass burning emissions. Anthropogenic emissions for the year 2001 were largely based on the EDGAR3.2 dataset [*Olivier and Berdowski*, 2001], and biomass burning emissions were based on *van der Werf et al.* [2003] (Table S2; also for a comparison with RCP 2000 emissions).

[14] Although anthropogenic and biomass burning emissions are unchanged between present and future, all the models use interactive lightning NO_x emissions according to *Price and Rind* [1992, 1994] and *Price et al.* [1997] which are sensitive to changes in cloud top height in a future climate. The CCMs simulate future increases in lightning NO_x emissions ranging from 0.75 to 1.49 Tg N/yr (11–26%), and these increases are most prominent over S. America, Africa, and S. Asia (Figure S3). The STOC-HadAM3 model employs an interactive climate-sensitive isoprene emission scheme [*Guenther et al.*, 1995] and gives a 22% global-mean increase in isoprene emissions due to climate change. Monoterpene emissions which may also be sensitive to climate were not interactive in the STOC-HadAM3 simulations. Isoprene emissions remained fixed in the other two CCMs, reflecting uncertainty in the extent to which CO_2 inhibition of isoprene emissions in a future higher CO_2 climate may counteract temperature-driven increases. For example, *Heald et al.* [2009] find that increases in future isoprene emissions due to a projected warmer climate are entirely offset by including the CO_2 inhibition effects. In a future 2090s climate under the SRES A2 climate scenario with corresponding atmospheric CO_2 levels, *Young et al.* [2009] find either small increases or decreases (depending on location) in isoprene emissions when CO_2 inhibition effects are included. However, there may also be an indirect effect of higher CO_2 that enhances isoprene emission through increased leaf area index (LAI) [*Guenther et al.*, 2012].

[15] These experiments termed "2000base" and "2095base" have the same setup as the control SR1 simulations reported in *Fiore et al.* [2009] and *TF-HTAP* [2011], apart from differing climate conditions (Table 1). An addition to these simulations was the inclusion of artificial CO-like tracers in STOC-HadAM3 and UM-CAM. These tracers are emitted from anthropogenic CO sources and have a first-order decay lifetime of 50 days [*Shindell et al.*, 2008; *Fang et al.*, 2011; Schultz et al., 2013, in preparation]. One CO tracer was emitted from each HTAP source region. These tracers enable diagnosis of how changes in transport from source regions affect the distributions of trace gas species with similar lifetimes (such as CO and O_3) between present day and future. The differences between the 2000base and 2095base experiments are used to gauge the potential impacts of climate change on surface O_3 and its precursors as well as on tracer transport.

[16] To study the impact of climate change on O_3 source-receptor (S-R) relationships, a further set of simulations was performed by the three CCMs (Table 1). These simulations focused on intercontinental transport between four major emission regions: North America (NA), Europe (EU), East Asia (EA), and South Asia (SA) as defined in *Fiore et al.* [2009], (hereafter termed the HTAP emission source regions) depicted in Figure 2a. For each of the four source regions, simulations were performed in which anthropogenic emissions of the O_3 precursors NO_x, NMVOCs, and CO were simultaneously reduced by 20%. These simulations were performed for both the 2000s and 2095 climates and are labeled by the region where emissions were reduced (e.g., 2000em_NA). Differences between the 2000em and 2000base simulations for each source region give an estimate of the response of O_3 and its precursors to a 20% emission reduction over that region in a 2000 climate. The 20% regional perturbation was chosen to produce a clear O_3 reduction but yet to allow near-linear scaling to other perturbation sizes up to about 60% [*Fiore et al.*, 2009; *Wild et al.*, 2012].

[17] Since methane concentrations were fixed in all experiments, it is the short-term response of O_3 to the changes in emissions that is diagnosed rather than any longer term O_3 response due to changes in methane lifetime resulting from OH changes [e.g., *West et al.*, 2009; *Fiore et al.*, 2009].

2.2. Model Evaluation for Present-Day Surface O_3

[18] *Fiore et al.* [2009] compared simulated O_3 in year 2001 from 21 models to observations over the United States, Europe, and Japan. Here Figure 1 shows how present-day 5 year mean (2000–2005) surface O_3 simulated in the "2000base" experiment by the three CCMs used in this study (shown as solid colored lines) compares with observations and with the results from the 21 models in *Fiore et al.* [2009]. The three CCMs used here were also included in *Fiore et al.* [2009] (shown as dashed colored lines in Figure 1), but note that GISS-PUCCINI used different driving meteorology (NCEP reanalysis in *Fiore et al.* [2009] versus meteorology from a free-running GCM in this study) so small differences may be expected. Nonetheless, it can be seen that the 1 year (2001) and 5 year (2000–2005) mean O_3 results from these three CCMs are fairly similar (Figure 1).

[19] Overall, the seasonality of O_3 simulated by the CCMs for the different locations lies well within the range simulated by the full set of models. The results from GISS-PUCCINI are nearer the lower end of the simulated O_3 range in some regions, while STOC-HadAM3 on some occasions overestimates O_3 compared to observations. GISS-PUCCINI exhibits a low O_3 bias particularly in summer months for the Mediterranean, the Central and South Europe, and the SW United States, although there is an improvement in the 5 year mean compared to the 2001 results for SW United States. However, its lower summer values in NE and SE United States are more in line with observations. The NMVOC emissions used by GISS-PUCCINI are lower than for the other two CCMs used here (Table S2) and compared to the ensemble-mean value of 630 Tg C yr^{-1} from *Fiore et al.* [2009]. This may in part explain the low O_3 simulated by

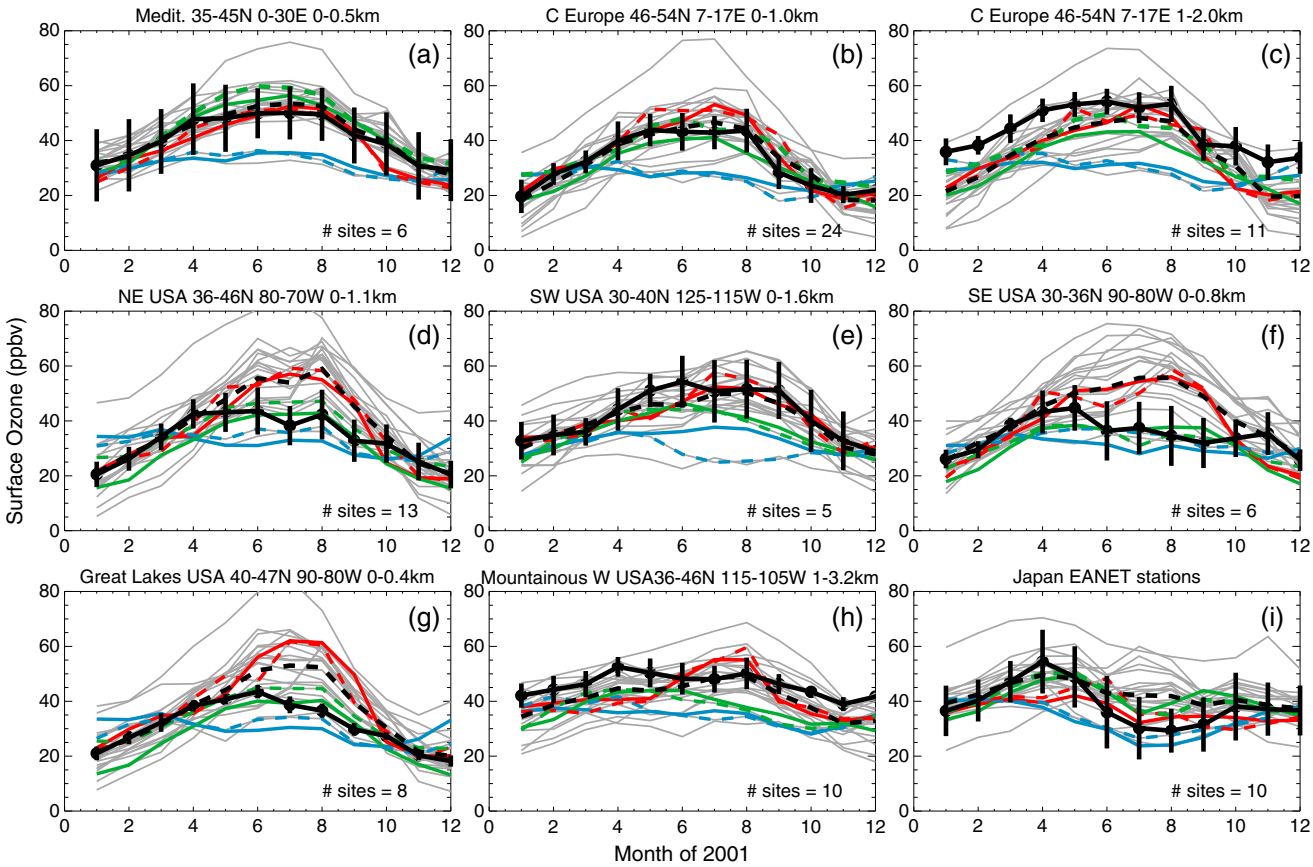

Figure 1. Monthly average surface O_3 observations (ppbv) for the year 2001 (solid black line; vertical bars represent one standard deviation) reproduced from *Fiore et al.* [2009, Figure 2], which describes full details of the observations (CASTNET, EMEP, and EANET). The multi-model ensemble mean of monthly average O_3 for 2001 from 21 models is shown with a black dashed line, and results from individual models are shown with gray lines. Monthly average surface O_3 from the three CCMs applied in this study (GISS-PUCCINI: blue, STOC-HadAM3: red, and UM-CAM: green) are shown for 2001 as in *Fiore et al.* [2009] (dashed colored lines) and for the 5 year mean from the 2000base experiment (solid colored lines).

GISS-PUCCINI. UM-CAM typically simulates O_3 to within one standard deviation of the observations except in central Europe (Figure 1c) and for summer and autumn in SW and W United States. STOC-HadAM3 typically overestimates O_3 in summer in NE and SE United States and in the Great Lakes compared to observations, like the multi-model ensemble mean. Overall, the current three CCMs provide a representative sample of the full set of models used in *Fiore et al.* [2009] in terms of their present-day O_3 simulation in 2001 as shown in Figure 1. It is noted that the transport in STOC-HadAM3 and UM-CAM is similar since these two CCMs use the same AGCMs (section 2.1) but that the chemistry schemes are entirely independent (Table S1).

2.3. Chemistry-Focused Sensitivity Simulations

[20] To aid interpretation of the overall O_3 response to climate change which results from a number of competing effects, sensitivity experiments were performed with STOC-HadAM3 to isolate the O_3 response to key chemical reactions and processes particularly sensitive to climate. Three prominent effects of climate change on surface O_3 summarized by *Jacob and Winner* [2009] in their comprehensive review were investigated: enhanced PAN thermal decomposition (simulation 2000PAN), enhanced water vapor concentrations (2000H2O), and enhanced isoprene emissions (2000ISO) along with the combined effect of all three (2000COM); see Table 1.

[21] These 5 year sensitivity simulations were carried out relative to the 2000base simulation. The difference between these simulations and 2000base provides an estimate of the change in surface O_3 due to each individual process. The similarity between the spatial pattern of change in surface O_3 to each perturbed process (and the combination of processes) and the surface O_3 response due to climate change is quantified using a Pearson correlation (since a linear relationship was found between the two spatial datasets in all cases). The intention is to assess the relative importance of each process in different regions and the extent to which the combination of these three effects reproduces the net climate change effect on surface O_3.

[22] In the "2000PAN" experiment, the average change in global-mean surface temperature of +3K across the three CCMs due to climate change (as derived from multi-model mean 2095base-2000base) was added throughout the model

domain to the temperature used in the calculation of the PAN decomposition rate:

$$PAN + M \rightarrow CH_3COO_2 + NO_2 + M \quad (R1)$$

[23] The decomposition rate increases very rapidly with temperature. For the reaction rate coefficients utilized in STOC-HadAM3, an increase in surface temperature from 287K to 290K decreases the lifetime of PAN from ~4 to 2.5 h, and at ~425 hPa, an increase in temperature from 250K to 253K decreases the PAN lifetime from ~6 to 3 months. The 2000PAN and the other sensitivity simulations do not account for the temperature and humidity change varying with altitude. However, the zonal-mean temperature and humidity increases due to climate change in the CCMs lie within the range of 3–5K and 15–30%, respectively, and are largely uniform with altitude in the lower and middle troposphere. The temperature increases due to climate change are about 1K larger over land than ocean (Figure S4), and hence, using the global-average temperature change over the model domain in these sensitivity simulations will underestimate the effect of climate change due to temperature over land and overestimate the effect over the oceans. Humidity increases due to climate change are more uniform over land and ocean (Figure S4).

[24] In the "2000H2O" simulation, the global average +19% surface increase in specific humidity was imposed throughout the troposphere. Increasing water vapor has a strong effect on O_3 destruction through the reaction:

$$O(^1D) + H_2O \rightarrow 2OH \quad (R2)$$

[25] Increasing HO_x also increases O_3 destruction by direct reaction with O_3. R2 is the primary source of OH radicals, and an increase in OH can either enhance O_3 formation (through oxidation of NMVOCs, CH_4, and CO) or suppress it (through increased NO_2 to nitric acid (HNO_3) conversion) [*Jacob and Winner*, 2009].

[26] In the "2000ISO" experiment, a +3K temperature change was applied to the calculation of isoprene emissions from vegetation (the vegetation distribution remains fixed between present and future). This simple approach does not account for the effects on future isoprene emissions of CO_2 inhibition of emissions, changes in land cover, soil moisture or cloud cover, or future changes in land-use patterns. In STOC-HadAM3, isoprene emissions are related to temperature based on *Guenther et al*. [1995]. The emissions also depend on photosynthetically available radiation (PAR), but the climate sensitivity of this is not investigated here. In the scheme used, isoprene emission increases rapidly with temperature up to a maximum at 314K. A 3K increase in surface temperature from present day values produces a 17% increase in global isoprene emission.

[27] The individual perturbations (+3K to PAN decomposition and isoprene emission and +19% increase to water vapor) were applied together in the "2000COM" experiment to assess the linearity of the surface O_3 response to these processes acting simultaneously. Finally, a further set of simulations were performed using the above simulations as a baseline and applying 20% anthropogenic emission reductions of O_3 precursors in the NA source region only.

3. Climate Change Impact on Surface O_3 and Its Precursors

[28] Annual-mean surface O_3 distributions for present-day (2000–2005) in all three CCMs highlight the northern mid-latitude emission and outflow regions where surface O_3 concentrations are high (Figure 2, top row). However, the spatial patterns of surface O_3 across the globe are somewhat variable across the three CCMs; e.g., only STOC-HadAM3 exhibits very high annual-mean surface O_3 in the southern hemisphere, which may be partly due to the higher NMVOC natural emissions in this CCM. However, differences in model chemistry and transport are also important since natural NMVOC emissions in UM-CAM are only about 25% lower than in STOC-HadAM3 (Table S2). In contrast, natural NMVOC emissions in GISS-PUCCINI are substantially lower than that in the other two models which may explain the lower surface O_3 concentrations in GISS-PUCCINI over the northern mid-latitude continents. Lower surface O_3 over the N. Atlantic in STOC-HadAM3 is likely due to differences in transport and deposition over oceans. The high surface O_3 concentrations over the Tibetan plateau and over Greenland in GISS-PUCCINI (also seen in UM-CAM) are most probably due to higher stratosphere-troposphere exchange (STE) than in STOC-HadAM3. Overall, while differences in emissions account for some of the differences in simulated O_3 between the three CCMs, differences in the representation of model chemistry and transport processes are likely to be the main source of these differences.

[29] The annual-average surface O_3 response to the warm climate in 2095–2099 relative to 2000–2005 shows characteristic features described in previous studies [e.g., *Hauglustaine et al*., 2005; *Murazaki and Hess*, 2006; *Zeng et al*., 2008]: reduced surface O_3 concentrations in less polluted regions and enhanced surface O_3 concentrations in some polluted areas in all three CCMs (Figure 2, bottom row). Very similar spatial patterns of surface O_3 response (and patterns of statistical significance) were found when the STOC-HadAM3 and UM-CAM simulations were extended to cover two 10 year periods (2000–2009 and 2090–2099) (Figure S5). These results further confirm that 5 years is sufficient in these simulations to capture the climate change signal in surface O_3 in all the CCMs.

[30] Higher water vapor concentrations lead to reduced surface O_3 in less polluted regions, causing a consistent decrease in background O_3 over most of the Earth's surface in the CCMs [*Thompson et al*., 1989; *Johnson et al*., 1999, 2001; *Murazaki and Hess*, 2006]. In polluted regions (delineated very approximately by the 500 ppt NO_x contours for the 2000 climate in Figure 2), the response is more mixed. Increased surface O_3 (up to 6 ppbv) occurs over considerable parts of the major emission source regions in GISS-PUCCINI and STOC-HadAM3 (Figures 2d–2e) but is confined to small areas in the UM-CAM simulations (Figure 2f). In the northern mid-latitudes, southern Europe and northeastern United States are the only regions where all CCMs consistently simulate O_3 increases. Overall, the three CCMs exhibit some areas of O_3 increase in the high NO_x regions, but the spatial patterns of O_3 increase in the three CCMs exhibit considerable variability in terms of their location and extent. A multi-model study using regional chemistry transport models also shows substantial variability in climate change-induced patterns of surface O_3 increase over the

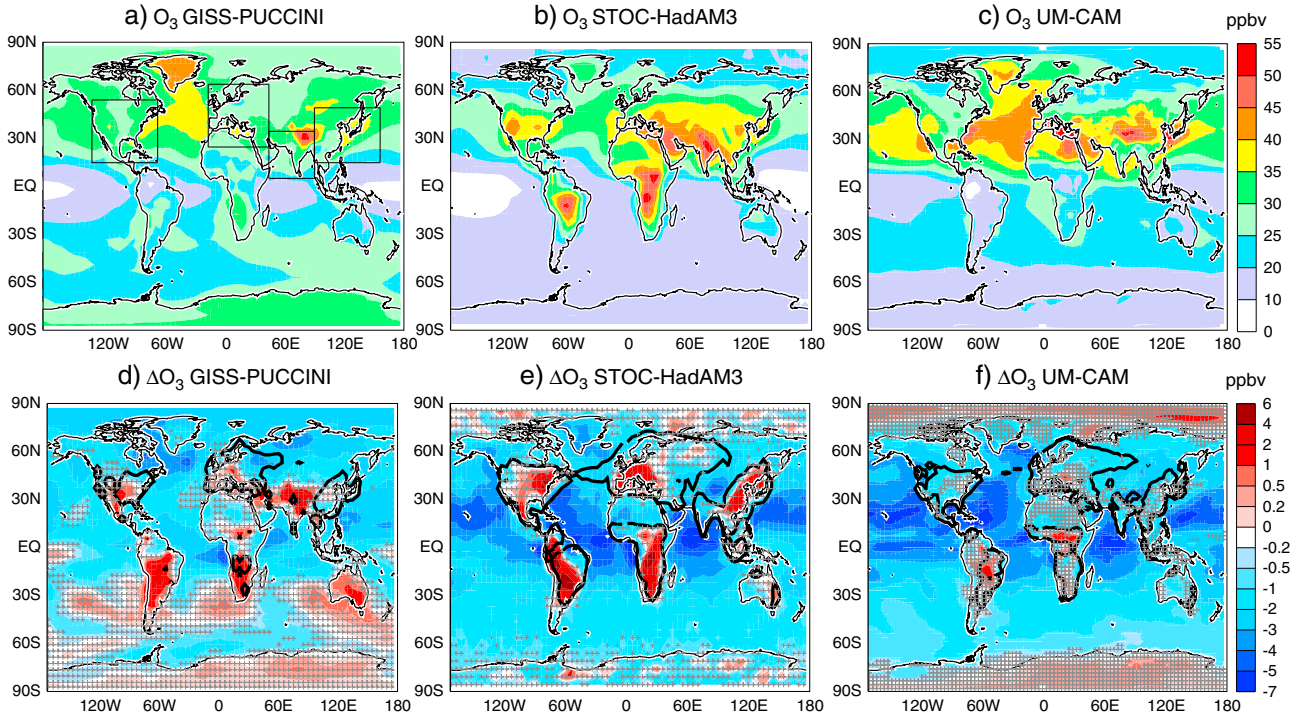

Figure 2. Top row: 5 year annual-average surface O_3 concentrations (ppbv) (2000base) for (a) GISS-PUCCINI, (b) STOC-HadAM3, and (c) UM-CAM. Bottom row: The difference in the 5 year mean annual-average surface O_3 concentrations (2095base–2000base) for the same three CCMs (d–f). The 500 pptv contour of NO_x surface concentrations for the 2000base simulation (thick black line) is used as an approximate indicator of polluted regions. Hatched areas, denoted by the + symbol, indicate where results are not significant at the 0.05 level as evaluated with a Student *t*-test using 5 years of data for the 2095 and 2000 climate simulations. The HTAP source regions are depicted in Figure 2a: NA (15°N–55°N; 60°W–125°W), EU (25°N–65°N; 10°W–50°E), EA (15°N–50°N; 95°E–160°E), and SA (5°N–35°N; 50°E–95°E).

United States [*Weaver et al.*, 2009]. Dilution of emissions over polluted regions due to the relatively coarse model resolution may result in a lesser sensitivity to climate change than would be given by higher resolution models. The strong O_3 increase over the S. Hemisphere continents in STOC-HadAM3 is likely primarily due to increased isoprene emission in these regions. Increased lightning NO_x emissions over these regions may also influence surface O_3 concentrations especially for GISS-PUCCINI (Figure S3). The strong O_3 increase simulated by GISS-PUCCINI over Tibetan plateau is likely related to enhanced STE in the future climate (Figure 2d). It is noted that the areas of O_3 increases from southern hemisphere continental outflow regions depicted for GISS-PUCCINI are not significant.

[31] The season of maximum surface O_3 for the 2000 climate generally agrees with the season of maximum surface O_3 derived from 2001 results (T. Nagashima, personal communication, 2012), although in some northern parts of the mid-latitude continents, GISS-PUCCINI shows maximum surface O_3 in winter due to the influx of stratospheric air. The spatial patterns of the season of maximum surface O_3 for the present-day within the four HTAP emission source regions vary typically between spring and summer across the CCMs; only in parts of the United States and in southern EU is summer (JJA) consistently the season of maximum O_3 (Figure S6). The three CCMs again all consistently show O_3 decreases during the season of maximum O_3 but with areas of O_3 increase in polluted northern mid-latitude regions. Increases in surface O_3 due to climate change in the season of maximum surface O_3 reach up to 14 ppbv in parts of the HTAP source regions (Figure S6). Like the annual-mean surface O_3 response, in the season of maximum surface O_3, there is considerable variability in the spatial patterns of O_3 increase between the three CCMs due to climate change. Again, parts of the United States and southern Europe show consistent O_3 increases across the three CCMs. In a multi-model regional study, *Langner et al.* [2012] also find consistent mean surface O_3 increases over April–September in southern Europe.

[32] Overall, additional future emission controls would be needed to achieve a targeted level of O_3 concentrations in many areas within polluted regions, e.g., southern Europe and northeastern United States, since annual-average O_3 concentrations are up to 6 ppbv or 10% higher (up to 14ppbv higher for the season of maximum surface O_3) in 2095 than in 2000 due to climate change alone. However, the considerable spatial variability and variation in the magnitude of simulated O_3 increases in these CCMs preclude the quantification of broad regional O_3 abatement targets. Generally, larger O_3 increases of greater areal extent are simulated by STOC-HadAM3 (Figures 2 and S6); which is the only model to include a temperature-sensitive isoprene emission scheme (section 2.1). *Langner et al.* [2012] also find that out of four regional chemistry transport models, the model with the

Table 2. Regional Average Change in 5 Year Annual-Average Surface Meteorology and Chemistry Variables (2095base–2000base)[a]

Surface Variable	Future (2095) Minus Present-Day (2000) Change in Annual-Mean Variable Averaged Over a HTAP Region			
	NA Region	EU Region	EA Region	SA Region
Temperature	4.4 (3.8–5.4)°C	4.7 (4.1–5.4)°C	4.2 (3.7–4.7)°C	4.6 (3.8–5.0)°C
Specific humidity	19.2 (19.1–19.2)%	20.6 (20.5–20.6)%	23.9 (20.7–27.0)%	24.6 (19.3–29.8)%
Precipitation	−4 (−10 to +0.6)%	−17 (−8 to −22)%	12 (7–14)%	22 (20–25)%
Fraction land area with O_3 increases	30 (2–47)%	33 (10–46)%	26 (2–53)%	25 (3–67)%
O_3	−2.2 (−1.4 to −3.4)%	−1.0 (−2.0 to +0.4)%	−1.6 (−2.9 to +0.2)%	−3.0 (−8.2 to +2.2)%
PAN	−30 (−24 to −42)%	−32 (−22 to −44)%	−25 (−20 to −34)%	−37 (−35 to −39)%
OH	12 (2–18)%	11 (7–15)%	13 (9–16)%	9 (5–12)%
HNO_3	0.8 (−5.6 to +5.0)%	2.7 (1.0-5.2)%	8.0 (−3.1 to 19.3)%	7.9 (0.2 to 22.2)%
NO_x	−1.8 (−0.1 to −4.3)%	−6.0 (−3.7 to −8.1)%	−0.1 (−2.7 to 1.2)%	−0.7 (−2.4 to +2.0)%
HNO_3 wet deposition	0.4 (−9 to +7)%	−17 (−14 to −19)%	14 (11–22)%	20 (12–28)%
C_5H_8 emission[b]	40%	31%	51%	10%
Net O_3 production (P-L)	13 (4–19)%	19 (7–33)%	7 (0.4–16)%	3 (0.3–6)%
O_3 dry deposition	−3.4(−0.2 to −9.4)%	−0.05 (−1.2 to +1.1)%	−1.1 (−4.8 to +2.2)%	0.1 (−10.3 to +11.0)%

[a]Only land grid boxes are included in the averaging. Values represent the mean value across the three CCMs, with the individual model ranges given in parenthesis.
[b]This variable is only available for STOC-HadAM3.

largest isoprene emission change has the greatest sensitivity in its O_3 response to climate change. Enhanced isoprene emissions in high NO_x emission regions (where O_3 production is VOC limited) can substantially augment O_3 levels [e.g., *Racherla and Adams*, 2008] and is likely to be the dominant mechanism producing future O_3 increases in the STOC-HadAM3 CCM. This is investigated further in section 5.

[33] The influence of climate change on the O_3 chemical environment was also investigated for the four HTAP emission source regions (Table 2). Regional annual-average values were calculated within each HTAP region for land only. In each HTAP region, the fraction of land showing surface O_3 increases is typically around one third, averaged across the three CCMs (Table 2). Overall, regional-wide annual-average surface O_3 generally decreases slightly (1–3%) (Table 2) in all four HTAP regions.

[34] *Sillman and Samson* [1995] suggest that O_3 increases with temperature in polluted regions largely because of an increase in PAN decomposition (R1). The production of PAN ties up NO_x and reduces the source of peroxy radicals, which then can be subjected to long-range transport in the form of PAN [*Murazaki and Hess*, 2006]. Across the four regions, higher temperatures in the future (4.2–4.7°C) yield substantial decreases in PAN (25–37%) (Table 2) (in agreement with *Hauglustaine et al*. [2005]) and increases in hydroxyl radical (OH) concentrations. Higher water vapor mixing ratios (19–25%) also elevate OH (R2) (9–13%), which promotes O_3 formation but also converts NO_2 to HNO_3 that is rapidly rained out to remove NO_x and suppress further O_3 formation [*Jacob and Winner*, 2009]. Accordingly, HNO_3 generally increases (1–8%), leading to a reduction in the lifetime of NO_x. Hence, unlike some previous studies [e.g., *Murazaki and Hess*, 2006], here PAN decreases are typically accompanied by small NO_x decreases or little change (0.1–6%) (Table 2) rather than NO_x increases across these source regions. This finding is however consistent with *Racherla and Adams* [2008] who report NO_x decreases (and HNO_3 increases) associated with lower $NO:NO_2$ ratios in high O_3 regions across the eastern half of the United States in a future climate. Across the four HTAP regions, lower $NO:NO_2$ ratios (0.5–4%) are simulated in future both in STOC-HadAM3 and UM-CAM (the only CCMs this ratio is available for). Changes in wet deposition of HNO_3 vary in sign depending on region and are not consistently related to changes in HNO_3 concentrations across the four regions but typically reflect the changing patterns of rainfall (Table 2).

[35] In the warmer future climate, increases in isoprene emission in the four regions range from 10 to 50% in STOC-HadAM3, further promoting O_3 formation in these high NO_x emission regions. This result is reported in numerous other studies [e.g., *Racherla and Adams*, 2008; *Zeng et al*., 2008; *Jacob and Winner*, 2009]. Despite surface O_3 decreases, in all three CCMs, the changes in O_3 chemistry described above lead to enhanced O_3 chemical production and loss in the source regions such that net chemical production of O_3 (chemical production (P)-chemical loss (L)) increases by 3–19% (Table 2). Another potentially important O_3 budget term is O_3 dry deposition. However, changes in O_3 deposition in these four source regions vary in sign across the CCMs, probably reflecting differences in model deposition schemes (e.g., inclusion of stomatal conductance) and near-surface meteorology (Table S1). The regional surface O_3 response to climate change therefore appears dominated by the lowering of background O_3 concentrations in a future climate which outweighs the increased regional net O_3 chemical production (P-L). The lower regional-average surface O_3 and higher O_3 loss rate also imply a decrease in the O_3 lifetime near the surface. *Racherla and Adams* [2008] also find increases in surface net chemical production and decreases in surface O_3 lifetime over the eastern United States.

[36] In summary, temperature and water vapor changes perturb NO_y, HO_x, and O_3 chemistry through a number of complex interactions described above. The relative contributions of temperature-dependent PAN decomposition (R1) and isoprene emission changes, as well as water vapor (R2) increases to surface O_3 change, are assessed in section 5.

4. The Relationship Between Surface O_3 and Surface Temperature Change

[37] In this section, the variability in surface O_3 increase projected by the different CCMs due to climate change is explored in further detail. High-O_3 events in high emission regions often show a strong relationship with temperature

due to either chemistry processes or O_3 precursor emissions sensitive to climate (section 5) or associated with stagnation episodes [*Jacob and Winner*, 2009; *Rasmussen et al.*, 2012]. Here, the dependence of the relationship between the change in surface O_3 with temperature and underlying NO_x concentrations is quantified for the three CCMs for the three mid-latitude HTAP regions: NA, EU, and EA. The analysis covers the months May to September which are typically the months of peak O_3 for these regions (Figure S6).

[38] Due to the substantial sub-regional variability in O_3 change over the large HTAP regions (Table 2), these three regions were divided into four sub-regions with equal latitude and longitude ranges. The SA region was not included because of its differing seasonal cycle of surface O_3 (e.g., minima in JJA). Sub-regional averages for present-day NO_x (2000–2005), ΔO_3 (2095–2099 minus 2000–2005), and ΔT (2095–2099 minus 2000–2005) were calculated from all the grid cells over land within the appropriate sub-region. The relationship between ΔO_3 and ΔT across all sub-regions, months, and years was then examined (sample size = 5 months × 5 years × 12 sub-regions = 300) (Figure 3). Positive relationships were found for all three CCMs, with the climate penalty (the increase in surface O_3 per 1°C increase in temperature) ranging between 0.34 and 1.20 ppbv (Figure 3, left panels), although the correlation coefficient only reached $r = 0.45$. The slopes were lowest for GISS-PUCCINI which also exhibits considerably lower mean NO_x levels than the other CCMs and highest for STOC-HadAM3.

[39] To assess the influence of NO_x on ΔO_3 /ΔT, the data were further divided into percentile ranges based on NO_x concentrations in each CCM. The relationship between ΔO_3 and ΔT was examined for the <25th, 25th–50th,

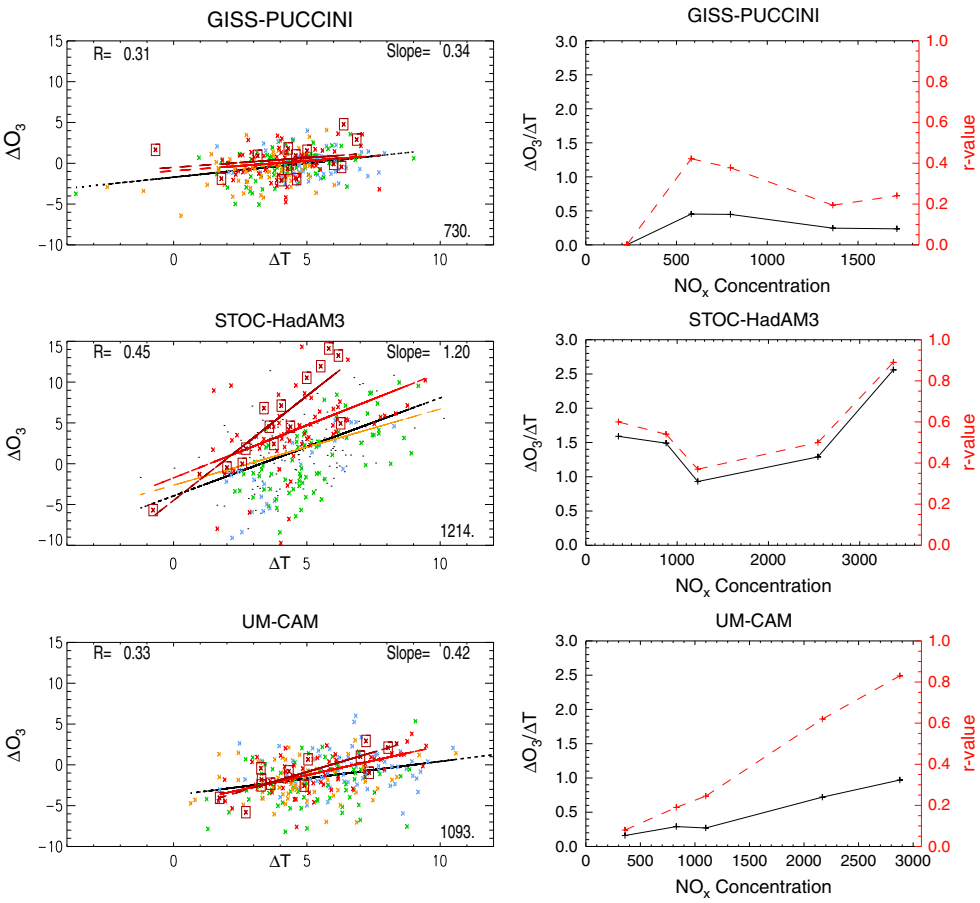

Figure 3. Left-hand panels: Regional-average relationship between monthly ΔO_3 versus ΔT (2095–2000 climates) for each CCM for the three major mid-latitude source regions (NA, EU, and EA) for the peak O_3 months of May–September over all 5 years in each climate period (black line). Each point represents 1 month in one of 5 years in each sub-region The data are color-coded by percentile category based on NO_x concentration in the 2000s (orange = NO_x concentration in the 50th–75th percentile; bright red = NO_x concentration above the 75th percentile; dark red = NO_x above the 95th percentile). The linear fit for ΔO_3 versus ΔT was calculated for data that fell into each percentile, and each curve uses the same color coding. The slope value using all the data points is given at the top right of each panel, and the regional average NO_x concentration (pptv) is given at the bottom right. Squares show the >95th percentile values that emanate from the EU region. Right-hand panels: the change in the slope of $\Delta O_3/\Delta T$ and correlation coefficient (r) for each NO_x percentile 0–25th, 25–50th, 50th–75th, 75th–100th, and 95th–100th with the x axis showing the NO_x concentrations mid-way across the respective percentile range. Note the different x axis ranges for each CCM.

50th–75th, >75th, and >95th percentiles. In all three CCMs, all NO_x values in the >95th percentile category, bar one point, are from the EU region (Figure 3, left panels).

[40] No clear relationship between the gradient of ΔO_3 and ΔT, and NO_x level is exhibited for GISS-PUCCINI. For the other two CCMs, the gradient of $\Delta O_3/\Delta T$ steepens progressively for data in the 50th–75th and higher percentile categories. Accordingly, the correlation coefficient is greater for these higher percentile categories (Figure 3, right panels). The NO_x concentrations in these higher percentile ranges are also substantially larger in STOC-HadAM3 and UM-CAM compared to GISS-PUCCINI. For the >95th percentile data, the slope of $\Delta O_3/\Delta T$ and the mean NO_x concentration are much higher in STOC-HadAM3 than in UM-CAM although the small sample size at this highest NO_x level precludes definitive conclusions. Largely similar results are found when the analysis is repeated with deseasonalized data.

[41] To test the robustness of these results, a set of linear mixed statistical models [*Pinheiro and Bates*, 2000] were constructed to examine the association between simulated ΔO_3 and ΔT from each of the three CCMs. The effects of NO_x, month, and region were considered, as were potential interactions between these variables and ΔT. Statistical models that included or excluded these variables were compared using Akaike's Information Criterion (AIC) [*Burnham and Anderson*, 2002]. All of the statistical models also contained random effects for year, location, a year-by-location interaction, and a year-by-month interaction in order to avoid pseudo-replication by accounting for spatial and temporal dependence [*Hurlbert*, 1984].

[42] AIC provides a way of assessing the performance of statistical models by balancing the goodness-of-fit of the model (as measured by the maximum value of log-likelihood function, l) against the complexity of the model (as measured by the number of parameters in the model, p) and is defined to be $\mathrm{AIC} = -2l + 2p$. Statistical models with lower AIC values have better performance than models with high AIC values; the statistical model with lowest AIC can be regarded as being the best supported model, but models with AIC values close to this (typically AIC values within two units of the best model) [*Burnham and Anderson*, 2002] can also be regarded as having good empirical support. The best supported models (the statistical models with the lowest AIC values for each CCM) are listed in Table 3.

[43] For all three CCMs there is strong evidence of a relationship between ΔO_3 and ΔT. Alternate statistical models that excluded ΔT were very poorly supported according to AIC. Hence, variations in ΔO_3 cannot be explained solely by differences between months, regions, and NO_x levels. For GISS-PUCCINI, the optimal statistical model for ΔO_3 is based on ΔT as a predictor alone (Table 3). For STOC-HadAM3, the best statistical model indicates that the magnitude of the $\Delta O_3/\Delta T$ relationship is dependent upon the NO_x level and upon month (since the model contained interaction terms between ΔT and NO_x percentile and between ΔT and month). For UM-CAM, the best statistical model also shows an interaction between ΔT and NO_x percentile. The best statistical models for STOC-HadAM3 and UM-CAM also contain an effect for "region," suggesting that overall ΔO_3 values differ between regions but do not include an interaction between region and ΔT (suggesting that the strength of the ΔT-ΔO_3 relationship does not vary between regions). Alternative models with good empirical support for ΔO_3 from STOC-HadAM3 and UM-CAM all contained ΔT and a dependence on NO_x percentile. For GISS-PUCCINI, no alternate model was well supported. In summary, the results suggest that the slope of $\Delta O_3/\Delta T$ is influenced by NO_x level for UM-CAM (most strongly) and for STOC-HadAM3 but not for GISS-PUCCINI, which has substantially lower mean NO_x levels.

Table 3. Best Statistical Model for ΔO_3 Based On AIC Criteria

CCM	Best Statistical Model
GISS-PUCCINI	$\Delta O_3 = \Delta T$
STOC-HadAM3	$\Delta O_3 = \Delta T \times NO_x$ class $+ \Delta T \times$ month $+$ region
UM-CAM	$\Delta O_3 = \Delta T \times NO_x$ class $+$ region

[44] Overall, the results from STOC-HadAM3 and UM-CAM suggest that the sensitivity of surface O_3 increases to temperature change is highest in the EU region due primarily to its high NO_x levels. However, the slopes derived from the three CCMs here are generally lower than those derived from perturbation studies over polluted regions (>2 ppbv per 1°C increase) [*Jacob and Winner*, 2009], but these typically use higher order O_3 metrics than monthly mean O_3 and consider smaller-scale urban regions. *Rasmussen et al.* [2012] also find modeled slope values of monthly average daily O_3/T within two out of three regions in the eastern United States are lower in summer months compared to observations (their Figure 6). Steeper O_3/T and $\Delta O_3/\Delta T$ gradients with higher NO_x levels have also been previously reported. *Bloomer et al.* [2009] find a larger climate penalty (in this case, the slope of hourly O_3 /T within four regions in the eastern U.S.) prior to 2002 when NO_x emissions were considerably larger than that in later years. *Wu et al.* [2008] report a decrease in the climate penalty, defined as ΔO_3 between 2050 and 2000, over the United States (their Figure 9), under a reduced (~40%) NO_x emission scenario. Therefore, the modification of $\Delta O_3/\Delta T$ by NO_x percentile range, shown by two of the three CCMs, is in broad agreement with the findings of these above studies.

5. Chemical Processes Determining the Climate Change Impact on Surface O_3

[45] Results from sensitivity simulations with the STOC-HadAM3 CCM were used to determine the relative importance of different chemical processes, influenced by climate change, on surface O_3 changes. These sensitivity perturbations applied the difference in global-mean surface temperature (3K) or water vapor (19%) between the 2095 and 2000 climates as spatially uniform changes (section 2.3).

[46] A 3K increase in temperature applied to the PAN decomposition rate (R1) alone (2000PAN simulation) produces contrasting surface O_3 responses over land and ocean. Over land, surface O_3 concentrations increase by 0–2 ppbv in northern mid-latitude regions and by up to 6 ppbv in the tropics (Figure 4a). Changes in O_3 precursor concentrations and O_3 production for these simulations are shown in Table 4 (for comparison with Table 2). Enhanced PAN decomposition leads to substantial decreases in surface PAN concentrations across the HTAP regions (25–32%), slight

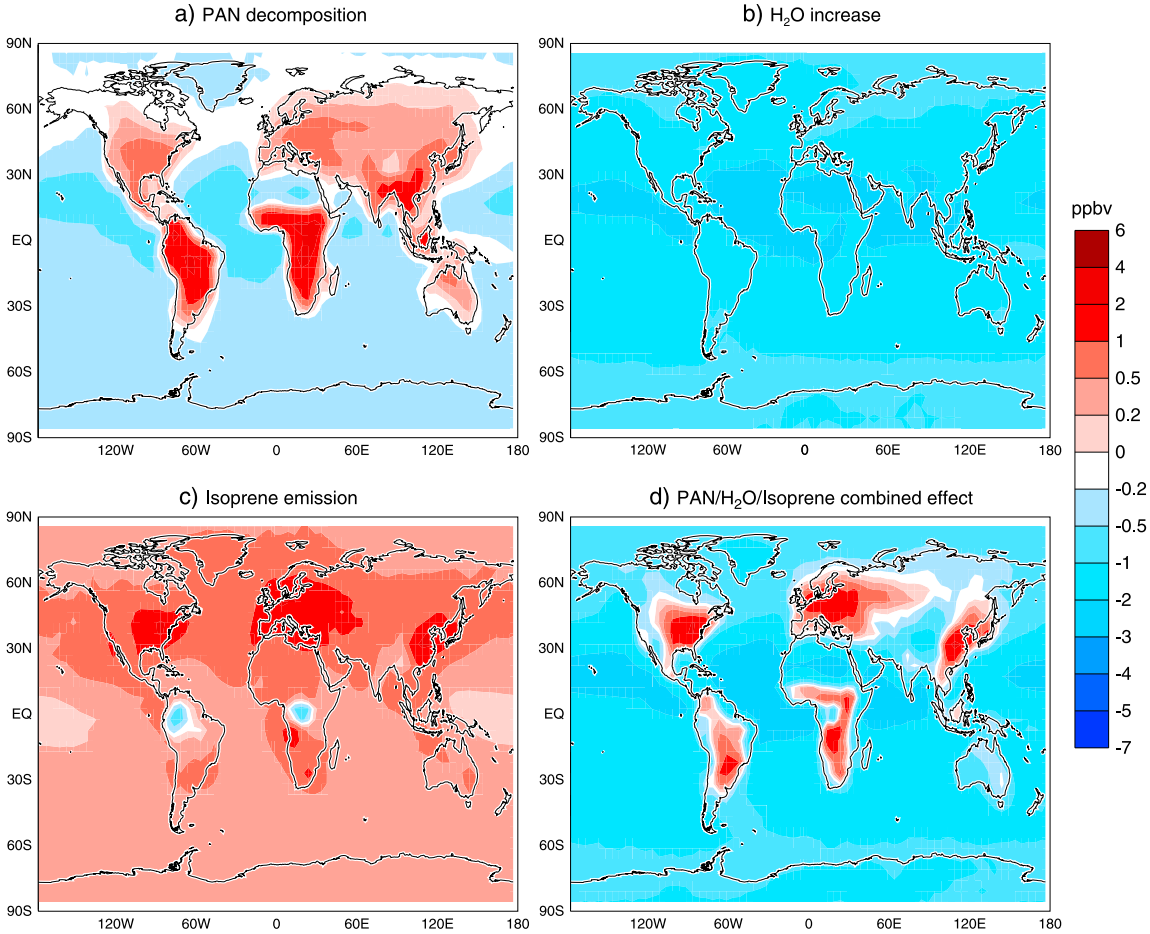

Figure 4. The difference in 5 year annual-average surface O_3 concentrations (ppbv) relative to 2000base for the following perturbations: (a) +3K to PAN decomposition rate (2000PAN), (b) 19% increase in water vapor mixing ratio (2000H2O), (c) +3K to isoprene emissions scheme (2000ISO), and (d) the combined effect (2000COM). Results are from the STOC-HadAM3 CCM only.

increases in surface OH, and increases in HNO_3 (2–4%). These regional-average changes are similar to those due to climate change except that the OH response is much smaller. Hence, the PAN and HNO_3 responses due to climate change can largely be attributed to increased PAN decomposition. Regional-average surface NO_x decreases slightly (except in EA) as seen under climate change. Regional-average net chemical O_3 production (1–6%) and surface O_3 concentrations (~1%) increase over land (Table 4).

[47] Less PAN transported from the emission regions leads to lower O_3 production downwind and to surface O_3 decreases of up to 1 ppbv over the tropical oceans (Figure 4a). Hence, the effect of temperature increases on PAN decomposition contributes both to surface O_3 enhancement in some parts of the HTAP source regions (~20–50% of the O_3 increases due to climate change) and O_3 decreases over the remote oceans (Figures 4a and 2b). The variability in the global spatial pattern of the O_3 response to climate

Table 4. Regional Annual-Average Change in Surface O_3, O_3 Precursors and Net O_3 Chemical Production Between the Perturbed and Base-Case Present-Day Simulations (2000PAN, H2O, ISO Minus 2000base)

Surface Variable	Perturbed Minus Present-Day Change in Annual-Mean Variable Averaged Over a HTAP Region (%)											
	NA Region			EU Region			EA Region			SA Region		
	PAN	H2O	ISO	PAN	H2O	ISO	PAN	H2O	ISO	PAN	H2O	ISO
O_3	1.0	−4.6	2.8	0.8	−3.9	3.2	1.6	−4.1	2.8	0.7	−5.4	1.3
NO_x	−0.2	−1.0	−1.8	−0.4	−1.2	−1.8	0.4	−1.1	−1.8	−0.5	−0.9	0.3
PAN	−29	−0.8	13	−27	−0.5	12	−25	−0.4	12	−32	−1.5	8
HNO_3	3.2	1.1	−2.0	2.1	0.9	−0.5	4.1	1.0	−2.8	2.1	0.3	−0.8
OH	1.6	5.8	−6.0	1.1	6.0	−3.3	2.1	5.9	−7.4	0.9	5.7	−2.6
Net O_3 Prod.(P-L)	5.9	2.8	7.3	2.9	2.0	8.3	5.1	1.0	5.6	1.0	−3.6	0.4
C_5H_8 emission			20			18			31			6

Only land grid boxes are included in the averaging.

change explained by the enhanced PAN decomposition alone is appreciable: $r^2 = 0.3$. In a further sensitivity simulation, +3K was applied to all chemical reaction rates. In this case, the O_3 response was very similar in pattern to that from PAN decomposition (R1) alone, but slightly smaller, with O_3 enhancements in northern mid-latitude source regions not typically exceeding 1 ppbv (Figure S7). This suggests that increased temperature augments both O_3 production (by enhancing PAN decomposition and OH oxidation of CH_4 and NMVOCs) and loss (by direct reaction of O_3, e. g., $O_3 + NO_2$). Overall, enhanced PAN decomposition (R1) is the primary driver of the O_3 response and its spatial pattern over land and ocean.

[48] The increase in water vapor concentrations alone, in 2000H2O, gives rise to increased O_3 destruction through (R2). Surface O_3 reductions of 1–2 ppbv occur globally and reach 3 ppbv across tropical locations (Figure 4b). In source regions, this decrease in surface O_3 partly offsets the O_3 increases caused by increased PAN decomposition. Across the four HTAP regions, the 19% increase in water vapor concentrations leads to uniform OH increases of ~6% (Table 4). Changes in net O_3 chemical production are generally positive but range from −4 to +3% depending on region. Surface O_3 concentrations decrease by 4–5% across these source regions. Therefore, higher water vapor concentrations in the 2095 climate relative to the 2000 climate are likely to be the primary cause of both the increase in OH and the decrease in surface O_3 concentrations at the regional level (Tables 2 and 4). Over ocean regions, the increase in water vapor explains ~50% of the surface O_3 decrease due to climate change. The variability in the global spatial distribution of O_3 response to climate change explained by enhanced water vapor is similar to that due to enhanced PAN decomposition ($r^2 = 0.29$).

[49] A 3K increase in temperature on isoprene emissions alone leads to O_3 increases over both land and ocean with the largest increases in the HTAP regions (~2ppbv) (Figure 4c). Enhanced isoprene emission only produces surface O_3 decreases in small areas of Amazonia and Central Africa where isoprene emissions are already high and NO_x levels are low. Across the four HTAP regions, isoprene emission increases by 6–31% (Table 4). Isoprene, as a NMVOC, is a major O_3 precursor under high NO_x conditions [*Jacob and Winner*, 2009] and also a precursor for PAN. Thus, isoprene affects the partitioning among oxidized nitrogen species, shifting the balance from HNO_3 towards PAN [*Horowitz et al.*, 1998; *Fiore et al.*, 2011]. Accordingly, across the four HTAP regions, enhanced isoprene emission substantially increases surface PAN concentrations (8–13%) and slightly reduces HNO_3. Surface OH concentrations are also reduced (3–7%) as noted in other studies [*Racherla and Adams*, 2008; *Zeng et al.*, 2008; *Fiore et al.*, 2011], and this contributes to reduced HNO_3 [*Racherla and Adams*, 2008]. There are increases in regional-average net chemical production of O_3 (up to 8%) and surface O_3 (1–3%). These surface O_3 increases account for ~40% of that due to climate change. Therefore, in these HTAP regions, the effect of temperature on isoprene emissions makes a larger contribution to increased surface O_3 than enhanced PAN decomposition (Table 4 and Figures 4a and 4c) for the STOC-HadAM3 CCM. However, these O_3 increases are larger than those simulated by *Fiore et al.* [2011] with a different model. Over the NA region, a +3K increase in surface temperature leads to a 20% increase in regional-average isoprene emission and a 2.8 ppbv increase in annual-average surface O_3 in STOC-HadAM3 (Table 4). *Fiore et al.* [2011] find that a uniform 20% isoprene emission increase over the NA region only increases monthly surface O_3 by up to 0.6 ppbv (see their Figure 4).

[50] Over the remote oceans, increased isoprene emission also leads to enhanced O_3, due to higher PAN concentrations [*Pfister et al.*, 2008; *Zeng et al.*, 2008, *Fiore et al.*, 2011]. Under climate change, these O_3 increases partly offset the O_3 decreases arising from increased water vapor and PAN decomposition. The insensitivity of isoprene emissions to temperature in the GISS-PUCCINI and UM-CAM simulations may therefore explain the smaller magnitude and areal extent of O_3 increases due to climate change in high NO_x regions than in the STOC-HadAM3 simulations (section 3). However, isoprene nitrate chemistry [*Fiore et al.*, 2005; *Horowitz et al.*, 2007; *Ito et al.*, 2009; *Archibald et al.*, 2010] and isoprene emission responses to increased temperature and atmospheric CO_2 concentrations, as discussed in section 2.1, remain highly uncertain.

[51] These sensitivity simulations illustrate the different influences on background O_3 (through PAN and H_2O changes) as well as on local O_3 levels (through OH and net O_3 chemical production changes) that contribute to the overall continental-scale O_3 response. The full climate change effect on surface O_3 is likely to be more complex than these three individual chemical effects. However, the combination of these effects on surface O_3 (Figure 4d) yields similar spatial patterns of change to that produced due to climate change (Figure 2b), r^2 value of 0.52. Furthermore, the sum of the surface O_3 response to the individual effects is very similar in spatial pattern and in magnitude (to within ± 0.2 ppbv) to the surface O_3 response to the combination of effects. However, the magnitude of the combined O_3 response is about 40% lower in the four HTAP regions than the response due to climate change (Figure 2d). One reason for this is that the regional-average surface temperature (3.7–5.4K) and humidity (19–30%) increases over the HTAP regions are substantially higher than the global-mean surface changes that were applied here (+3K for temperature and 19% for water vapor). Further sensitivity simulations were performed using the maximum regional-mean changes from the HTAP regions (+5.4K for temperature and 30% for water vapor; see Table 2). The O_3 responses were found to scale linearly from the global-mean change to the maximum regional-average changes to within ± 0.2 ppbv for the three effects. Furthermore, the combined effect of the maximum regional-mean changes produces O_3 increases of a similar magnitude to those due to climate change (Figure S8). Finally, transport processes will also influence background and regional O_3 responses to climate change, and these are discussed in the following section.

6. Transport Changes

[52] To investigate the influence of differences in transport between present-day and future climates, passive CO tracer species were utilized (section 2.2). The CO tracer emitted from the NA region (Figure 5a) is the focus of the discussion here.

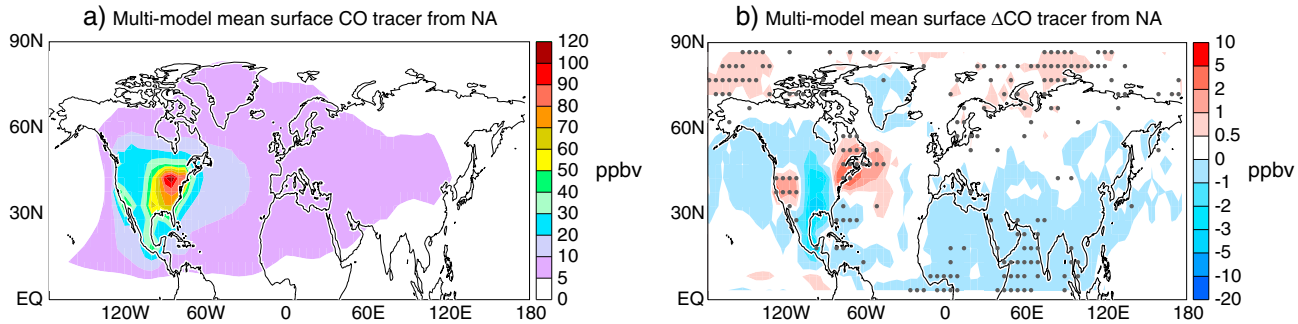

Figure 5. (a) Model-mean 5 year annual-average surface CO tracer concentrations (ppbv) for a species with a 50 day lifetime emitted as for CO over the NA source region from the STOC-HadAM3 and the UM-CAM CCMs (ppbv) for 2000 climate. (b) The difference in model-mean 5 year annual-average surface CO-tracer concentrations (ppbv) between the 2095 and 2000 climates. Both CCMs use the HadAM3 GCM driven by the same SSTs for their simulations. Dotted areas, denoted by the ● symbol, indicate where results are significant at a 0.05 level as evaluated with a Student *t*-test using 5 years of data for the 2095 and 2000 climate simulations.

[53] The STOC-HadAM3 and UM-CAM CCMs that include these CO-tracer species use the same climate model forced by the same SSTs for the present-day and future climate simulations (although there are different advection, convection, and boundary layer mixing schemes within the two chemistry transport models; Table S1). The model-mean annual-average response of the surface CO tracer from NA to climate change is displayed in Figure 5. In the 2095 climate, there is less (typically ~1–5% and up to 10%) of the annual-mean CO tracer from NA remaining at the surface in much of the NA source region than in the 2000 climate (Figure 5b), especially over the Great Plains region. This may suggest an enhancement of the low-level jet [*Murazaki and Hess*, 2006] and enhanced venting and export from the boundary layer in the future in that area. However, over the eastern and western United States and outflow regions, the CO tracer increases (Figure 5b) (0–10% and up to 25%) in the future suggesting reduced ventilation from the surface. Only the areas of CO-tracer increase are statistically significant at the 0.05 level (Figure 5) although at the 0.01 level, the area of CO-tracer decrease is significant. Similar spatial patterns of surface CO-tracer response were found between 2000 and 2095 when the STOC-HadAM3 and UM-CAM simulations were extended to cover two 10 year periods (2000–2009 and 2090–2099) and the areas of statistical significance at the 0.05 level included the areas of CO-tracer decrease in the Great Plains region. This suggests that the CO-tracer changes are robust and likely due to climate change.

[54] Overall, there appear to be complex shifts in transport that affect the surface distribution of the annual-mean CO-tracer response to climate change over NA and its outflow region, rather than any large-scale spatial response. Similar results were also found for CO-tracer species emitted from the other three HTAP regions (Figure S9), with distinct patterns of adjacent areas of lower and higher surface CO tracer concentrations that suggest a shift in circulation within all the regions that extends across the regional boundaries between present day and future. It is unlikely that these shifts in transport patterns have a major role in influencing the spatial patterns of at least the annual-mean O_3 response due to climate change. However, changes in transport may well be important when considering changes in higher moments of surface O_3 such as changes above the 95% percentile of O_3 or in daily 8 h maximum surface O_3.

[55] However, as these transport-related results are derived essentially from one GCM climate simulation, this precludes definitive statements about the robustness of the projected future changes in annual-mean CO tracer transport. *Fang et al.* [2011] consider the impact of climate change on CO-tracer transport using a tracer emitted globally with a 25 day lifetime in the GFDL AM3 model. They find a vertical redistribution of CO tracer in the future climate, which is also found here. However, *Fang et al.* [2011] find that surface zonal-mean CO tracer concentrations increase in the tropics and mid-latitudes in the future relative to present day. However, STOC-HadAM3 and UM-CAM simulate uniform increases in zonal-mean CO tracer only above ~800 hPa with mainly decreases below this pressure level. Therefore, CO-tracer transport changes may vary and depend on the representation of shallow convection processes in the individual models.

[56] In contrast to the mixed CO-tracer response to climate change over the HTAP regions found here, a number of previous studies have highlighted reduced boundary layer venting in a future climate over parts of the United States [*Mickley et al.*, 2004; *Murazaki and Hess*, 2006; *Leibensperger et al.*, 2008; *Wu et al.*, 2008] and W. Europe [*Hauglustaine et al.*, 2005; *Forkel and Knoche*, 2006]. *Racherla and Adams* [2008] suggest that different methodologies for analysis of synoptic-scale circulation changes may produce different results. Further process-based studies using a range of CCMs and methodologies are needed before more robust statements can be made concerning the effect of climate change on tracer transport.

7. Climate Change Impact on Ozone S-R Relationships

[57] In this section, the analysis is extended to consider O_3 S-R relationships and how these are modified due to climate change. Following the same approach as previous HTAP studies [*Fiore et al.*, 2009; *TF-HTAP*, 2011], O_3 S-R relationships were quantified by considering the O_3 response to a 20% reduction of O_3 precursors emissions

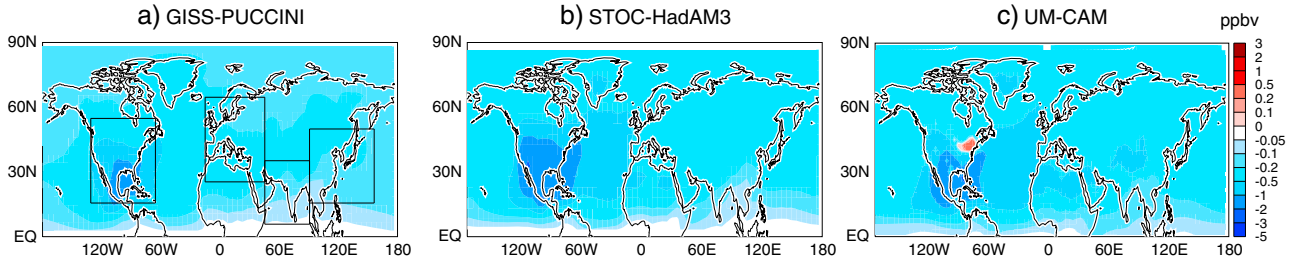

Figure 6. Impact of simultaneous 20% reductions of the O_3 precursor emissions (NO_x, NMVOCs, and CO) in the NA source region on 5 year annual-mean surface O_3 concentrations (ppbv) for 2000 climate for (a) the GISS-PUCCINI CCM, (b) STOC-HadAM3, and (c) UM-CAM (2000em_NA—2000base). The HTAP regions are depicted in Figure 6a).

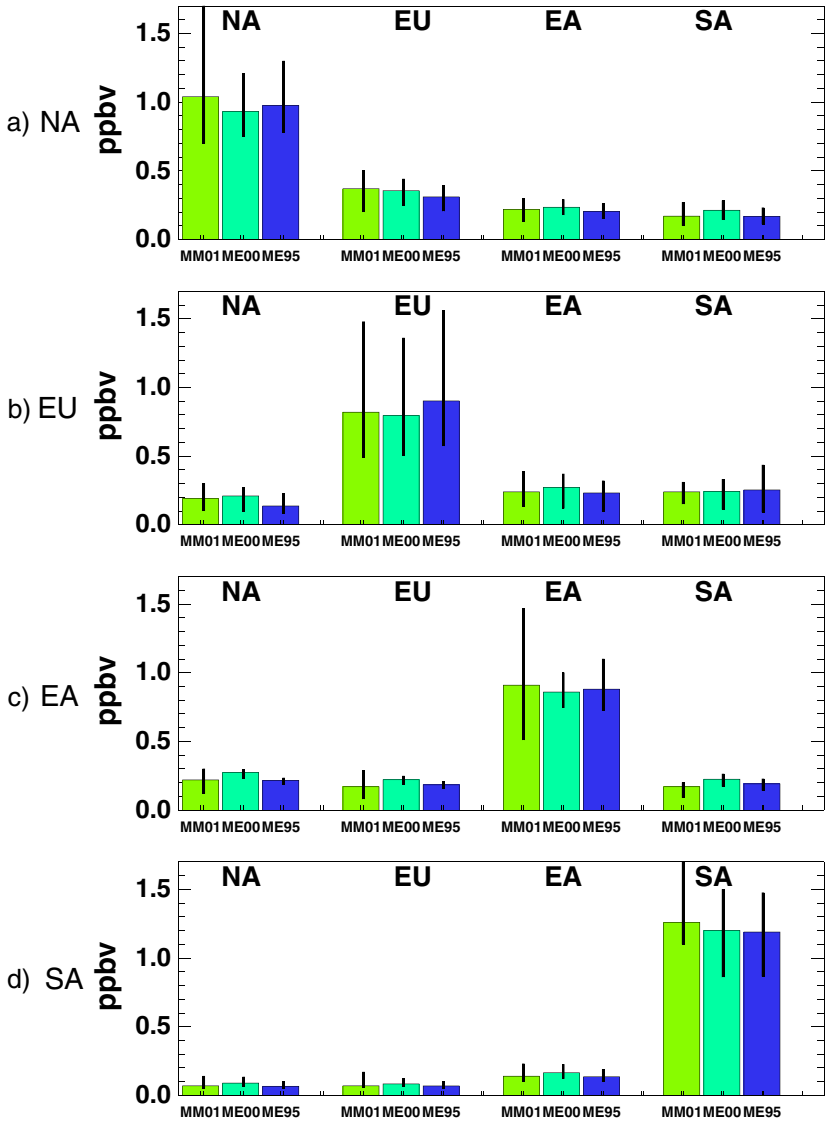

Figure 7. The reduction in regional-average annual-mean surface O_3 in the receptor region from 20% reductions in O_3 precursor emissions (NO_x, NMVOCs, and CO) in the (a) NA, (b) EU, (c) EA, and (d) SA source regions for the 2000 (00) and 2095 (95) climates. MM01 = Multi-model mean and ranges with 2001 climate [*Fiore et al.*, 2009]. ME00 = 3 model-mean and ranges for 2000 climate; ME95 = 3 model-mean and ranges for 2095 climate; for ME00 and ME95, results are 5 year mean averages. No land-sea mask is applied to the calculation of these area averages.

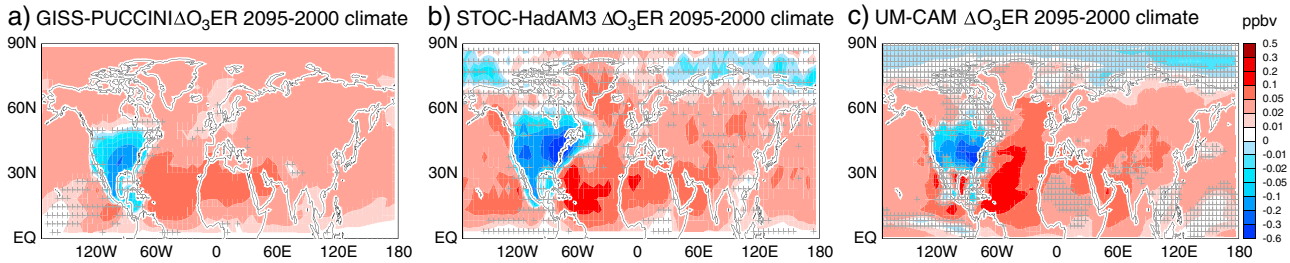

Figure 8. The difference in the impact of 20% reductions of O_3 anthropogenic precursor emissions over NA on 5 year annual-mean surface O_3 (ppbv) for the 2095 climate compared to the 2000 climate for the (a) GISS-PUCCINI, (b) STOC-HadAM3, and (c) UM-CAM CCMs (2095em_NA-2095base–2000em_NA-2000base). Hatched areas,denoted by the + symbol, indicate where results are not significant at the significance level of 0.05 as evaluated with Student *t*-test using 5 years of data for the 2095 and 2000 climate simulations. Negative values represent a larger reduction whilst positive values imply a lesser reduction in the O_3 response to emission reductions.

of NO_x, CO, and NMVOCs over a given source region, as compared to "no reduction" (section 2.1). The HTAP source regions discussed in the previous sections are now considered as both source and receptor regions for O_3 and its precursor emissions (Figure 6a). The NA source region is used for illustrative purposes in the next two sections.

[58] For present-day climate, in response to a 20% emission reduction of O_3 precursors over the NA region, all three CCMs simulate annual-mean surface O_3 decreases of 0.5–2ppbv (~2–10%) in the source region and up to 1ppbv (~3%) immediately downwind (Figure 6). Similar surface O_3 responses are found over the other three HTAP regions (Figures 7b–7d). The magnitude of the surface O_3 response simulated by GISS-PUCCINI is typically slightly less compared to the other two CCMs for all four HTAP source regions. The decreases in annual-mean surface O_3 over source and receptor regions simulated by all three CCMs for 2000 climate (ME00) (Figure 7) lie well within the multi-model range of results from the 15 models that participated in the sensitivity simulations for 2001 (MM01) (Figure 7) [*Fiore et al.*, 2009].

[59] The difference in the annual-mean O_3 response due to the 20% reduction of O_3 precursors in the NA region between the 2000 and 2095 climates is depicted for the three CCMs in Figures 7a and 8. When averaged over the large area of the HTAP regions, the difference in the surface O_3 response to emission reductions between the two climate periods is small (Figure 7). However, the differences in the spatial pattern of surface O_3 response to emission reductions between present-day and future climate is robust across the three CCMs (Figure 8) despite differences in their spatial patterns and magnitude of O_3 response to climate change (Figures 2d–2f).

[60] Across the three CCMs, the O_3 response to NA emission reductions in the future climate is consistently larger over the source region and smaller downwind compared to present-day climate, both in terms of absolute and relative changes. The annual-average surface O_3 response to the 20% NA emission reduction is enhanced by up to 0.6 ppbv (2%) in the NA source region and reduced by up to 0.2 ppbv (0.3%) immediately downwind (Figure 8). The regionally averaged annual-mean surface O_3 response to emission reductions is larger by 0.1 ppbv for the NA source region and smaller by ~0.05 ppbv and ~0.03 ppbv for the EU and EA receptor regions respectively (Figure 7a) in the future climate.

[61] Equivalent emission reduction simulations for the three other source regions yield similar results, with a greater surface O_3 response to a 20% emission reduction in the source region and a reduced response in downwind continents in the future compared to present-day climate (Figures 7b–7d). Over the SA region, the effect of large-scale averaging over land and downwind ocean leads to cancelation effects; hence, there is little difference in the regional O_3 response to emission reductions between the two climate periods (Figure 7d). In addition, the effect of emission reductions in the SA source region has a smaller influence on its three receptor regions compared to the influence of the other source regions on their respective receptor continents (Figure 7). This reflects the smaller region size and the more southerly location of this region such that SA pollution remains isolated from mid-latitude air [*Fiore et al.*, 2009]. Across all source and receptor regions, there is little interannual variation (<0.02 ppbv in the source regions; not shown) in the difference in the surface O_3 response between the two 5 year climate periods.

[62] The seasonality of the O_3 response to the reduction of O_3 precursors remains similar for the two climate periods in both the source and receptor regions (Figure S10) in the three CCMs. Over the source region, the EU shows the largest changes in magnitude of the O_3 response between the two periods in all three CCMs. There is little evidence of a consistent change in the peak month(s) of intercontinental transport between source and receptor regions, or in the frequency of underlying transport (e.g., storm track and flow patterns) between months, or in the seasonality of chemical transformation processes (e.g., O_3 lifetime) between the two climate periods. Thus, climate change has little influence on the seasonality of the O_3 response to 20% emission reductions. This result is consistent with *Fiore et al.* [2011] who found the seasonality in the O_3 response to 20% decreases in NA anthropogenic emissions was unaltered when isoprene emissions were elevated.

8. Chemical Processes Influencing the Climate Change Impact on Surface O_3 S-R Relationships

[63] The climate-sensitive chemical processes discussed in section 5 are re-considered here in the context of how they

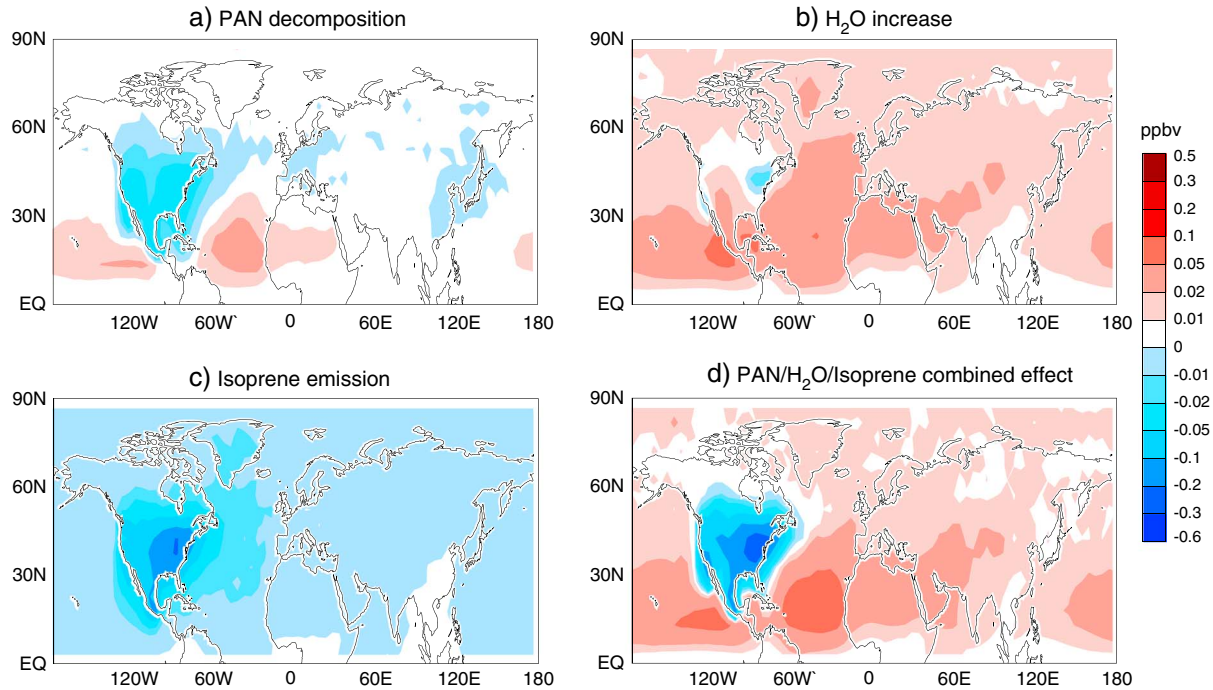

Figure 9. The difference in the impact of 20% reductions of O_3 precursor emissions over NA on 5 year annual-mean surface O_3 (ppbv) relative to 2000base for the following perturbations: (a) +3K to PAN decomposition rate (e.g., 2000PANem_NA-2000PAN–2000em_NA-2000base), (b) 19% increase water vapor mixing ratio, (c) +3K to isoprene emissions scheme, and (d) the combined effect. Results from the STOC-HADAM3 CCM only. Negative values represent an enhanced reduction, whilst positive values imply a lesser reduction in the O_3 response to emission reductions.

influence the annual-average O_3 response to O_3 precursor emissions reductions over the NA region (Figure 9).

[64] The difference in the surface O_3 response to 20% NA emission reductions of O_3 precursors between the sensitivity simulations with increased temperature applied to the PAN decomposition (R1) alone (2000PANem_NA-2000PAN) and the base (2000em_NA-2000base) simulations (Figure 9a) shows a similar spatial pattern to that due to climate change (Figure 8b) ($r^2 = 0.5$). There is a greater O_3 response to emission reductions in the source region but a lesser response downwind (Figure 9a). However, the difference in the O_3 response is smaller than that due to climate change. Under higher water vapor concentrations alone, only a small part of the NA source region shows an enhanced surface O_3 response, and there is a smaller O_3 response elsewhere in the source region and downwind (Figure 9b). This downwind O_3 response to emission reductions for higher water vapor concentrations alone is ~50% of the magnitude of that due to climate change (Figures 8b and 9b). In contrast, under elevated isoprene emission arising from a uniform +3K increase in temperature, there is a greater O_3 response to 20% anthropogenic emission reductions in both source and receptor regions (Figure 9c). These differences in the absolute O_3 response largely reflect the changes in surface O_3 concentration that occur under these different perturbation simulations.

[65] The three processes thus have competing effects on the O_3 S-R response to emission reductions in both the NA source and receptor regions. For the source region, the temperature effect on isoprene emission influences the surface O_3 response more than PAN decomposition. In the downwind region, there is a reduced surface O_3 response due largely to water vapor effects but also to increased PAN decomposition. The combined effect of the three processes produces a spatial pattern of O_3 response to emission reductions which is similar to that due to climate change (Figures 9d and 8b) ($r^2 = 0.76$), but the magnitude is somewhat smaller. However, scaling to the maximum regional-mean temperature and humidity changes for these three effects yields O_3 responses similar in magnitude to those due to climate change.

9. The Impact of Climate Change Versus Emission Reductions on Surface O_3

[66] Given that climate change increases surface O_3 in some areas within major emission source regions, a key question for policy makers is how effective current air quality legislation will be in the future. The percentage change in region-wide O_3 precursor emissions required to balance the localized impact of climate change (i.e., at each CCM grid point) on annual-average surface O_3 concentrations over each HTAP region is shown in Figure 10. This is based on the parameterization of *Wild et al.* [2012] which provides an estimate of regional O_3 responses based on regional precursor emission changes scaled quadratically from the 20% emission reductions of NO_x, CO, and NMVOCs applied in the HTAP studies. This approach reproduces the nonlinear behavior of regional O_3 responses well for emission reductions of up to about 60%, and therefore, the focus here is on changes up to this magnitude to minimize the associated uncertainty. For simplicity, we assume that the emissions of

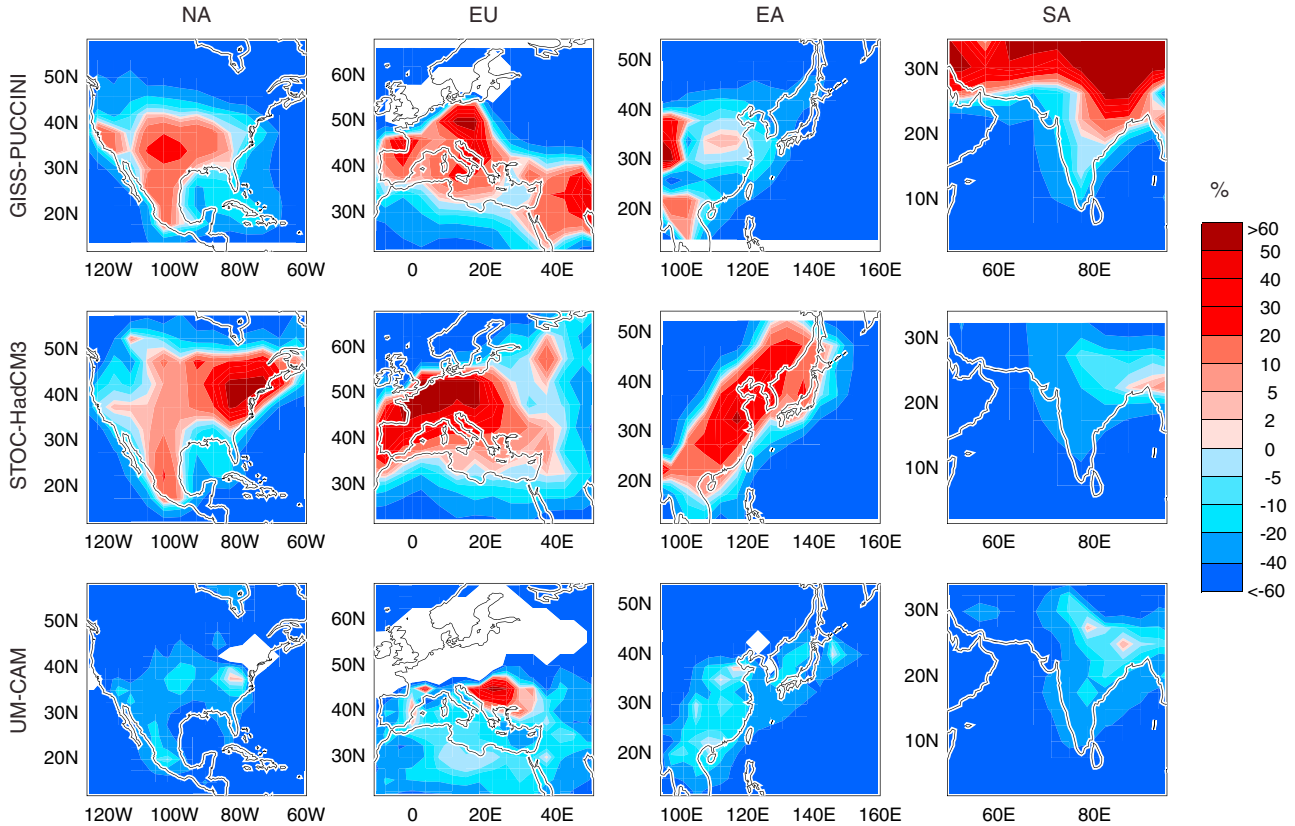

Figure 10. The percentage reduction in region-wide O_3 precursor emissions (NO_x, NMVOCs, and CO) required to counteract the impact of climate change (2095base-2000base) on 5 year annual-average surface O_3 concentrations over each HTAP region. This is calculated by dividing the impact of 2095–2000 climate change on surface O_3 by the effect of 20% regional O_3 precursor emission reductions on surface O_3 and multiplying the result according to the parameterization of *Wild et al*. [2012] (e.g., by 20% for a linear scaling). Each row shows a different model, and each column shows a different source region. Negative values (in blue) show where climate change leads to a reduction in O_3 and therefore where emissions can increase to maintain present-day (2000s) O_3 levels. Areas are shaded white when 20% regional emission reductions lead to increased O_3.

each of the different O_3 precursors are altered proportionally. Positive values (in red) show areas within the HTAP regions where regional emission reductions are necessary to overcome the increases in surface O_3 due to climate change such that present-day O_3 levels are retained. The spatial pattern of required regional emission change within each HTAP region varies considerably with CCM. This predominately reflects the variation in the annual-mean O_3 response due to climate change rather than variability in the O_3 response to regional O_3 precursor emission reductions. Although all HTAP regions show areas where regional emission reductions of more than 20% are required to balance annual-average surface O_3 increases due to climate change, this result is most consistent across the CCMs for the EU region. Within this region, there are large areas where regional emission reductions of more than 20% are required to balance the impact of climate change between 2095 and 2000 on annual-average surface O_3 concentrations (Figure 10), and reductions of more than 60% are required in some places. For the SA region, only the results from GISS-PUCCINI suggest that substantial regional emission reductions would be required to mitigate the localized effects of climate change across the Tibetan plateau (via enhanced STE) on the annual-mean O_3 response (Figures 10 and 2d). Larger regional emission reductions are generally required in STOC-HadAM3 to overcome climate change than in the other two CCMs. Again, this reflects the greater O_3 response to climate change in STOC-HadAM3 which may emanate from the temperature control on biogenic emissions that is only simulated in this CCM.

10. Conclusions

[67] This study examines the impact of climate change on surface O_3 and its precursors and on intercontinental transport of O_3 from major emission regions to downwind receptor continents. It further explores the relative contributions of key processes in producing this O_3 response. Three CCMs (GISS-PUCCINI, STOC-HadAM3, and UM-CAM) simulate surface O_3 concentrations for 2000 and 2095 climates as projected under the SRES A2 climate forcing scenario with current and reduced emissions of anthropogenic O_3 precursors. To isolate the effects of climate change, anthropogenic and biomass burning emissions and methane concentrations are fixed at 2000 levels.

[68] In the three CCMs, annual-mean surface O_3 generally decreases due to climate change but increases in parts of the more polluted regions, consistent with previous studies. Surface O_3 increases in high NO_x regions are up to 6 ppbv in the annual average and up to 14 ppbv in the season of present-day maximum surface O_3. This climate penalty effect on surface O_3 within the high NO_x regions is highly variable across the CCMs in location and spatial extent. The largest areas and magnitudes of O_3 increase are simulated by STOC-HadAM3, the only CCM that incorporates temperature-sensitive isoprene emission. Annual regional-mean surface O_3 decreases slightly (1–3%) in conjunction with substantial PAN decreases (~30%) and elevated OH (~10%) and HNO_3 levels across the four HTAP regions. This shift in NO_y partitioning from PAN to HNO_3 under climate change is in agreement with previous studies [e.g., *Zeng et al*., 2008; *Racherla and Adams*, 2008].

[69] The relationship between monthly (May–September) surface O_3 change (ΔO_3) and temperature change (ΔT) is quantified in order to explore how the climate penalty relates to NO_x concentrations. Positive $\Delta O_3/\Delta T$ relationships are exhibited by all three CCMs and the gradient of $\Delta O_3/\Delta T$ steepens with increased NO_x percentile class in UM-CAM (most strongly) and STOC-HadAM3. Consequently, in UM-CAM and STOC-HadAM3, the sensitivity of surface O_3 increase to temperature change is greatest in the EU region, where all three CCMs simulate the highest NO_x concentrations. The lack of variation in $\Delta O_3/\Delta T$ with NO_x percentile class for GISS-PUCCINI may reflect its lower NO_x concentrations.

[70] The relative importance of three chemical processes that affect O_3 chemistry and are sensitive to temperature and humidity changes (PAN decomposition, water vapor concentrations (hence HO_x), and isoprene emission) is examined in further simulations using the STOC-HadAM3 CCM. An increase in temperature acting only on the PAN thermal decomposition rate leads to surface O_3 increases over land and decreases over ocean. Increased water vapor mixing ratios lead to O_3 decreases everywhere. In contrast, enhanced isoprene emission due to higher temperature yields surface O_3 increases over most locations. Given this potential importance of future changes in isoprene emission further research is needed to quantify uncertainties in isoprene nitrate chemistry and the influence of temperature and CO_2 effects on isoprene emissions [e.g., *Guenther et al*., 2012]. Other climate-sensitive emissions such as methane from wetlands [e.g., *Shindell et al*., 2006] and NO_x from soils [e.g., *Zeng et al*., 2008] also merit further study. Although the climate change impact on surface O_3 is likely to be more complex than the sum of individual chemical effects, it is found that the combination of these three effects largely reproduces the spatial patterns of annual-mean O_3 response due to climate change ($R^2 = 0.52$).

[71] The impact of climate change on transport is evaluated with an idealized CO-like tracer species emitted from all four major source regions. Over all four HTAP regions, annual-mean CO-tracer concentrations exhibit distinct dipole patterns of increase and decrease in future compared to present-day climate that suggest subtle shifts in transport within the region and its area of outflow, rather than any consistent large-scale pattern. It is unlikely that these complex shifts in regional circulation exert a substantial control on the coherent spatial pattern of the annual-mean surface O_3 response to climate change; hence, the simulated annual-mean surface O_3 response to climate change arises predominately from changes in chemistry. However, the effect of climate change on transport may well depend on model representation of shallow convection processes. Further process-based studies are required to quantify how climate change affects the transport of chemical constituents.

[72] The impact of climate change on intercontinental transport of O_3 is also considered through source-receptor (S-R) relationships that quantify the impact of changing anthropogenic emissions in a source region on surface O_3 both within and beyond that region. A small but robust difference in the annual-mean surface O_3 response to a 20% reduction in O_3 anthropogenic precursor emissions (NO_x, CO, and NMVOCs) between the present day and future climate is simulated by all three CCMs. The O_3 response to regional emission reductions is larger over the source region and smaller downwind in the future climate over all four HTAP regions. There is no change in the seasonality of the O_3 response to emission reductions in either the source or receptor regions. The combination of the surface O_3 response to emission reductions under (i) enhanced PAN decomposition, (ii) higher water vapor mixing ratios, and (iii) elevated isoprene emission, relative to the O_3 response to emission reductions under present-day climate, is similar to that due to climate change ($R^2 = 0.76$).

[73] Overall, this study suggests that the dominant effects of mean climate change on annual-mean O_3 and its intercontinental transport are via temperature and water vapor effects on the chemical environment rather than climate-related changes in transport. Changes in transport may well be important when considering changes in peak O_3 events.

[74] The regional emission reduction required to balance the impact of climate change such that present-day annual-mean surface O_3 levels are retained is calculated across the four HTAP regions. The required emission change within each HTAP region varies considerably with CCM; typically larger values are projected by STOC-HadAM3, the CCM with temperature-sensitive isoprene emission. All three CCMs consistently show areas within the EU region where substantial (>20%) regional emission reductions are required to balance climate change impacts on annual-mean surface O_3. This emphasizes that the impact of climate change must be accounted for in designing future emission policies at least for these four major emission regions. *Langner et al*. [2012] find that the spatial features of the change in daily maximum O_3 produced by climate change are similar to those for summer time average O_3. Hence, this current study focusing on annual and seasonal mean changes should be a useful guide for assessing the effects of climate change on policy-relevant O_3 metrics.

[75] **Acknowledgments.** We greatly thank Adam Butler for statistical expertise, advice, and insights. We are also extremely grateful to Owen Cooper for informal discussions and his review of the manuscript. We thank Paul Young and Larry Horowitz for insightful discussions. This work was performed under the Task Force on Hemispheric Transport of Air Pollution (www.htap.org). We thank the US EPA and European Commission for travel support to HTAP meetings. We also thank Michael Decker and Sabine Schröder for hosting the HTAP data repository at Forschungszentrum Juelich. GZ acknowledges NIWA HPCF facility and funding from New Zealand Ministry of Science and Innovation. RD and GZ thank Colin Johnson at the UK Met Office for provision of sea-surface temperature data, and RD thanks Lois

Steenman-Clark and Grenville Lister for supercomputing support. This work made use of the facilities of HECToR, the UK's national high-performance computing service, which is provided by UoE HPCx Ltd at the University of Edinburgh, Cray Inc and NAG Ltd, and funded by the Office of Science and Technology through EPSRC's High End Computing Program.

References

Akimoto, H. (2003), Global air quality and pollution, *Science*, *302*(5651), 1716–1719, doi:10.1126/science.1092666.

Andersson C., and M. Engardt (2010), European ozone in a future climate: Importance of changes in dry deposition and isoprene emissions, *J. Geophys. Res.*, *115*, D02303, doi:10.1029/2008JD011690.

Archibald, A. T., M. C. Cooke, S. R. Utembe, D. E. Shallcross, R. G. Derwent, and M. E. Jenkin (2010), Impacts of mechanistic changes on HO_x formation and recycling in the oxidation of isoprene, *Atmos. Chem. Phys.*, *10*, 8097–8118, doi:10.5194/acp-10-8097-2010.

Arneth, A., P. A. Miller, M. Scholze, T. Hickler, G. Schurgers, B. Smith and I. C. Prentice (2007), CO2 inhibition of global terrestrial isoprene emissions: Potential implications for atmospheric chemistry. *Geophys. Res. Lett. 34*, L18813, doi:10.1029/2007GL030615.

Bloomer, B. J., J. W. Stehr, C. A. Piety, R. J. Salawitch, and R. R. Dickerson (2009), Observed relationships of ozone air pollution with temperature and emissions, *Geophys. Res. Lett.*, *36*, L09803, doi:10.1029/2009GL037308.

Burnham, K. P., and D. R. Anderson (2002), Model Selection and Multimodel Inference: A Practical Information-Theoretic Approach, 2nd ed. Springer-Verlag, New York. ISBN 0-387-95364-7.

Fang Y., A. M. Fiore, L. W. Horowitz, A. Gnanadesikan, I. Held, G. Chen, G. Vechhi, and H. Levy (2011), The impacts of changing transport and precipitation on pollutant distributions in a future climate. *J. Geophys. Res. 116*, D18303, doi:10.1029/2011JD015642. 6/11.

Fiore, A. M., L. W. Horowitz, D. W. Purves, H. Levy II, M. J. Evans, Y. Wang, Q. Li, and R. M. Yantosca (2005), Evaluating the contribution of changes in isoprene emissions to surface ozone trends over the eastern United States , *J. Geophys. Res.*, *110*, D12303, doi:10.1029/2004JD005485.

Fiore, A. M., H. Levy II, and D. A Jaffe (2011), North American isoprene influence on intercontinental ozone pollution. *Atmos. Chem. Phys.*, *11*(4), doi:10.5194/acp-11-1697-2011.

Fiore, A. M., et al. (2009), Multimodel estimates of intercontinental source-receptor relationships for ozone pollution, *J. Geophys. Res.*, *114*, D04301, doi:10.1029/2008JD010816.

Fiore, A. M., et al. (2012), Global air quality and climate, *Chem. Soc. Rev.*, *41*(19), doi:10.1039/C2CS35095E.

Forkel, R., and R. Knoche (2006), Regional climate change and its impact on photooxidant concentrations in southern Germany: Simulations with a coupled regional chemistry-climate model, *J. Geophys. Res.*, *111*, D12302, doi:10.1029/2005JD006748.

Guenther, A., C. Hewitt, D. Erickson, R. Fall, C. Geron, T. Graedel, P. Harley, L. Klinger, M. Lerdau, and W. McKay (1995), A global model of natural volatile organic compound emissions, *J. Geophys. Res.*, *100*, 8873–8892, 1995, doi:10.1029/94JD02950, 1995.

Guenther, A. B., X. Jiang, C. L. Heald, T. Sakulyanontvittaya, T. Duhl, L. K. Emmons, and X. Wang (2012), The Model of Emissions of Gases and Aerosols from Nature version 2.1 (MEGAN2.1): An extended and updated framework for modeling biogenic emissions, *Geosci. Model Dev.*, *5*, 1471–1492, doi:10.5194/gmd-5-1471-2012.

Hauglustaine, D. A., J. Lathiere, S. Szopa, and G. A. Folberth (2005), Future tropospheric ozone simulated with a climate-chemistry-biosphere model, *Geophys. Res. Lett. 32*, L24807, doi:10.1029/2005GL024031.

Heald, C. L., M. J. Wilkinson, R. K. Monson, C. A. Alo, G. Wang, and A. Guenther (2009), Response of isoprene emission to ambient CO_2 changes and implications for global budgets, *Glob. Chang. Biol.*, *15*(4), 1127–1140.

Held, I. M., and B. J. Soden (2006), Robust responses of the hydrological cycle to global warming, *J. Clim.*, *19*(21), 14.

Holloway, T. A., A. Fiore, and M. G. Hastings (2003), Intercontinental transport of air pollution: Will emerging science lead to a new hemispheric treaty? *Environ. Sci. Technol. 37*, 4535–4542.

Horowitz, L. W., A. M. Fiore, G. P. Milly, R. C. Cohen, A. Perring, P. J. Wooldridge, P. G. Hess, L. K. Emmons, and J.-F. Lamarque (2007), Observational constraints on the chemistry of isoprene nitrates over the eastern United States, *J. Geophys. Res.*, *112*, D12S08, doi:10.1029/2006jd007747.

Horowitz, L. W., J. Liang, G. M. Gardner, and D. J Jacob (1998), Export of reactive nitrogen from North America during summertime: Sensitivity to hydrocarbon chemistry, *J. Geophys. Res.*, *103*, 13,451–13,476, doi:10.1029/97jd03142, 1998.

Hurlbert, S. H. (1984), Pseudoreplication and the design of ecological field experiments, *Ecological Monographs*, *54*(2), 187–211.

IPCC (2001), Climate Change 2001: The Scientific Basis, Contribution of Working Group I to the Third Assessment Report of the Intergovernmental Panel on Climate Change, edited by J.T. Houghton, Y. Ding, D. J. Griggs, M. Noguer, P.J. van der Linden, X. Dai, K. Maskell, and C. A. Johnson. Cambridge University Press, Cambridge, United Kingdom and New York, NY, USA, 881pp.

Isaksen, I. S. A., et al. (2009), Atmospheric composition change: Climate-chemistry interactions, *Atmos. Environ.*, *43*, 5138–5192, doi: 10.1016/j.atmosenv.2009.08.003.

Ito, A., S. Sillman, and J. E. Penner (2009), Global chemical transport model study of ozone response to changes in chemical kinetics and biogenic volatile organic compounds emissions due to increasing temperatures: Sensitivities to isoprene nitrate chemistry and grid resolution, *J. Geophys. Res.*, *114*, D09301, doi:10.1029/2008jd011254.

Jacob, D. J., and D. A. Winner (2009), Effect of climate change on air quality, *Atmos. Environ.*, *43*, 51–63, doi:10.1016/j.atmosenv.2008.09.051.

Johnson, C. E., W. J. Collins, D. S. Stevenson, and R. G. Derwent (1999), Relative roles of climate and emissions changes on future oxidant concentrations, *J. Geophys. Res.*, *104*(D15), 18631–18645, doi:10.1029/1999JD900204.

Johnson, C. E., D. S. Stevenson, W. J. Collins, and R. G. Derwent (2001), Role of climate feedback on methane and ozone studied with a coupled Ocean-Atmosphere-Chemistry model, *Geophys. Res. Lett.*, *28*, 1723–1726, doi:10.1029/2000GL011996.

Jonson, J. E., et al. (2010), A multi-model analysis of vertical ozone profiles, *Atmos. Chem. Phys.*, *10*, 5759–5783, doi:10.5194/acp-10-5759-2010.

Lang, C., and D. W. Waugh (2011), Impact of climate change on the frequency of Northern Hemisphere summer cyclones, *J. Geophys. Res.*, *116*, D04103, doi:10.1029/2010JD014300.

Langner, J., et al. (2012), A multi-model study of impacts of climate change on surface ozone in Europe, *Atmos. Chem. Phys.*, *12*, 10,423–10,440, doi:10.5194/acp-12-10423-2012, 2012.

Leibensperger, E. M., L. J. Mickley, and D. J. Jacob (2008), Sensitivity of U.S. air quality to midlatitude cyclone frequency and implications of 1980–2006 climate change, *Atmos. Chem. Phys.*, *8*, 7075–7086.

Lin, J.-T., et al. (2008), Effects of intercontinental transport on surface ozone over the United States: Present and future assessment with a global model, *Geophys. Res. Lett.*, *35*, L02805, doi:10.1029/2007GL031415.

Meinshausen, M., et al. (2011), The RCP greenhouse gas concentrations and their extensions from 1765 to 2300, *Clim. Chang.*, *109*, 213–241, doi:10.1007/s10584-011-0156-z.

Mickley, L. J., D. J. Jacob, B. D. Field, and D. Rind (2004), Effects of future climate change on regional air pollution episodes in theUnited States, *Geophys. Res. Lett. 30*, L24103, doi:10.1029/2004GL021216.

Murazaki, K., and P. Hess (2006), How does climate change contribute to surface ozone change over the United States?, *J. Geophys. Res.*, *111*, D05301, doi:10.1029/2005JD005873.

Nakicenovic, N., et al. (2000), IPCC Special Report on Emissions Scenarios, Cambridge University Press, Cambridge, UK and New York, NY.

Olivier, J. G. J., and J. J. M. Berdowski (2001), Global emissions sources and sinks, in: The Climate System, edited by Berdowski, J., Guicherit, R., and Heij, B. J., 33–78, A.A. Balkema Publishers/Swets and Zeitlinger Publishers, Lisse, The Netherlands, ISBN-90-5809-255-0, 2001.

Parrish, D. D., et al. (2012), Long-term changes in lower tropospheric baseline ozone concentrations at northern mid-latitudes, *Atmos. Chem. Phys.*, *12*, 11,485–11,504, doi:10.5194/acp-12-11485-2012.

Pfister, G. G., L. K. Emmons, P. G. Hess, J. F. Lamarque, J. J. Orlando, S. Walters, A. Guenther, P. I. Palmer, and P. J. Lawrence (2008), Contribution of isoprene to chemical budgets: A model tracer study with the NCAR CTM MOZART-4, *J. Geophys. Res.*, *113*, D05308, doi:10.1029/2007jd008948.

Pinheiro, J. C., and D. M. Bates (2000), Mixed-Effects Models in S and S-Plus, Springer, New York.

Price, C., and D. Rind (1992), A simple lightning parameterization for calculating global lightning distributions, *J. Geophys. Res.*, *97*, 9919–9933.

Price, C., and D. Rind (1994), Modelling global lightning distributions in a general circulation model, *Mon. Weather Rev.*, *122*, 1930–1939, 1994.

Price, C., J. Penner, and M. Prather (1997), NO_x from lightning: 1. Global distribution based on lightning physics, *J. Geophys. Res.*, *102*, 5929–5941.

Racherla, P. N., and P. J. Adams (2008), The response of surface ozone to climate change over the Eastern United States, *Atmos. Chem. Phys.*, *8*, 871–885, doi:10.5194/acp-8-871-2008.

Rasmussen, D., A. M. Fiore, V. Naik, L. W. Horowitz, S. J. McGinnis, and M. G. Schultz (2012), Surface ozone-temperature relationships across the eastern US: A monthly climatology for evaluating chemistry-climate models, *Atmos. Environ.*, *47*, 142–153, doi:10.1016/j.atmosenv.2011.11.021.

Rosenstiel, T. N., M. J. Potosnak, K. L. Griffin, R. Fall, and R. K. Monson (2003), Elevated CO_2 uncouples growth and isoprene emission in an agriforest ecosystem. *Nature*, *421*, 256–259.

Royal Society (2008), Ground-Level Ozone in the 21st Century: Future Trends, Impacts and Policy Implications. 148pp, The Royal Society, London.

Sanderson, M. G., C. D. Jones, W. J. Collins, C. E. Johnson, and R. G. Derwent (2003), Effect of climate change on isoprene emissions

and surface ozone levels, *Geophys. Res. Lett.*, *30*, 1936, doi:10.1029/2003GL017642.

Sanderson M. G., et al. (2008), A multi-model study of the hemispheric transport and deposition of oxidised nitrogen, *Geophys. Res. Lett.*, *35*, L17815, doi:10.1029/2008GL035389.

Schultz, M., R. Schmitt, K. Thomas, and A. Volz-Thomas (1998), Photochemical box modeling of long-range transport from North America to Tenerife during the North Atlantic Regional Experiment (NARE) 1993, *J. Geophys. Res.*, *103*(D11), 13,477–13,488.

Shindell, D. T., G. Faluvegi, N. Unger, E. Aguilar, G. A. Schmidt, D. M. Koch, S. E. Bauer, and R. L. Miller (2006), Simulations of preindustrial, present day, and 2100 conditions in the NASA GISS composition and climate model G-PUCCINI, *Atm. Chem. Phys.*, *6*, 4427–4459.

Shindell, D. T., et al. (2008), A multi-model assessment of pollution transport to the Arctic, *Atmos. Chem. Phys. 8*, 5353–5372.

Sillman, S., and P. J. Samson (1995), The impact of temperature on oxidant formation in urban, polluted rural and remote environments, *J. Geophys. Res.*, *100*(D7), 11497–11508, doi:10.1029/94JD02953.

Stevenson, D. S., F. J. Dentener, M. G. Schultz, et al. (2006), Multimodel ensemble simulations of present-day and near future tropospheric ozone, *J. Geophys. Res.*, *111*, D08301, doi:10.1029/2005JD006338, 2006.

Task Force on Hemispheric Transport of Air Pollution (TF-HTAP) (2007), Hemispheric Transport of Air Pollution 2010, Part A: Ozone and Particulate Matter, Air Pollut. Stud., 16, edited by: T. J. Keating, and A. Zuber, U. N. Econ. Comm. Eur., Geneva, Switzerland, available at: http://www.htap.org.

Task Force on Hemispheric Transport of Air Pollution (TF-HTAP) (2011), Hemispheric Transport of Air Pollution 2010, Part A: Ozone and Particulate Matter, Air Pollut. Stud., 17, edited by: F. Dentener, T. Keating, and H. Akimoto, U. N. Econ. Comm. Eur., Geneva, Switzerland, available at: http://www.htap.org.

Thompson, A. M., R. W. Stewart, M. A. Owens, and J. A. Herwehe (1989), Sensitivity of tropospheric oxidants to global chemical and climate change, *Atmos. Environ.*, *23*(3), 519–532.

Trainer, M., et al. (1991), Observations and modeling of the reactive nitrogen photochemistry at a rural site, *J. Geophys. Res.*, *96*(D2), 3045–3063, doi:10.1029/90JD02395.

Weaver, C. P., et al. (2009), A preliminary synthesis of modeled climate change impacts on U.S. regional ozone concentrations, *Bull. Amer. Met. Soc.*, *90*(12), 1843–1863, doi: 10.1175/2009BAMS2568.1.

van der Werf, G. R., T. J. Randerson, J. Collatz, and L. Giglio (2003), Carbon emissions from fires in tropical and subtropical ecosystems, *Global Change Biol.*, *9*, 547–562.

West, J. J., V. Naik, L. W. Horowitz, and A. M. Fiore (2009), Effect of regional precursor emission controls on long-range ozone transport—Part 2: Steady-state changes in ozone air quality and impacts on human mortality, *Atmos. Chem. Phys.*, *9*, 6095–6107.

Wild, O., et al. (2012), Future changes in surface ozone: A parametrized approach, *Atmos. Chem. Phys.*, *12*, 2037–2054, doi:10.5194/acp-12-2037-2012.

Wu, S., L. J. Mickley, J. O. Kaplan, and D. J. Jacob (2012), Impacts of changes in land use and land cover on atmospheric chemistry and air quality over the 21st century, *Atmos. Chem. Phys.*, *12*, 1597–1609, doi:10.5194/acp-12-1597-2012.

Wu, S., L. J. Mickley, E. M. Leibensperger, D. J. Jacob, D. Rind, and D. G. Streets (2008), Effects of 2000–2050 global change on ozone air quality in the United States, *J. Geophys. Res. 113*, D06302, doi:10.1029/2007JD008917.

Young, P. J., A. Arneth, G. Schurgers, G. Zeng, and J. A. Pyle (2009), The CO_2 inhibition of terrestrial isoprene emission significantly affects future ozone projections, *Atmos. Chem. Phys.*, *9*, 2793–2803.

Zeng, G., J. A. Pyle, and P. J. Young (2008), Impact of climate change on tropospheric ozone and its global budgets, *Atmos. Chem. Phys.*, *8*, 369–387.